

The Validity of Optical Properties as Tracers of Terrigenous Dissolved Organic Carbon during Extensive Remineralization in Coastal Waters

Yuan Chen¹, Patrick Martin², and YONGLI ZHOU²

¹Nanyang Technological University, Singapore

²Nanyang Technological University

September 11, 2023

1 **The Validity of Optical Properties as Tracers of Terrigenous Dissolved Organic**
2 **Carbon during Extensive Remineralization in Coastal Waters**

3 **Yuan Chen^{1,*}, Patrick Martin^{1,*}, and Yongli Zhou^{1,†}**

4 ¹ Asian School of the Environment, Nanyang Technological University, 639798, Singapore

5 [†]Present address: Marine Biological Laboratory, Woods Hole, MA 02543, USA

6

7 *Corresponding author:

8 Yuan Chen (yuan006@e.ntu.edu.sg) and Patrick Martin (pmartin@ntu.edu.sg)

9

10

11 **Key Points:**

- 12
- 13 • Chromophoric dissolved organic matter removal is more than terrestrial dissolved organic carbon (tDOC) remineralization in coastal water.
 - 14 • Commonly used optical properties can quantify percent tDOC in natural environment but
15 with different sensitivity.
 - 16 • None of the optical properties can indicate the extent of tDOC remineralization from
17 natural biogeochemical processing.
- 18

19 **Abstract**

20 Terrestrial dissolved organic carbon (tDOC) is significant for coastal carbon cycling, and
21 spectroscopy of chromophoric and fluorescent dissolved organic matter (CDOM, FDOM) is
22 widely used to study tDOC cycling. However, CDOM and FDOM are often amongst the more
23 labile components of tDOC. Because few studies have compared spectroscopy to measurements
24 of both bulk tDOC concentration and tDOC remineralization, it remains unclear how accurately
25 CDOM and FDOM actually trace tDOC in coastal waters when tDOC undergoes extensive
26 remineralization. We collected a 4-year coastal timeseries in Southeast Asia, where tropical
27 peatlands provide a large tDOC input. A carbon stable isotope mass balance shows that on average
28 56% of tDOC was remineralized upstream of our site, while 77% of CDOM was bleached. Despite
29 this extensive tDOC remineralization and preferential CDOM loss, optical properties could still
30 reliably quantify tDOC. CDOM spectral slope properties, such as $S_{275-295}$, are exponentially related
31 to tDOC; these are highly sensitive tDOC tracers at low, but not at high, tDOC concentrations.
32 Other properties are linearly related to tDOC, and both specific ultraviolet absorbance ($SUVA_{254}$)
33 and DOC-normalized fluorescence intensity may be suitable to quantify tDOC over a wider range
34 of concentrations. However, the optical properties did not show consistent changes with the extent
35 of tDOC remineralization. Our data support the validity of CDOM and FDOM spectroscopy to
36 trace tDOC across coastal gradients even after the majority of tDOC has been remineralized, but
37 they also show that these measurements may not provide direct information about the degree of
38 natural tDOC processing.

39 **1 Introduction**

40 Annually around 0.25 Pg C of terrestrial dissolved organic carbon (tDOC) are transported from
41 land to ocean, playing an important role in global and especially coastal carbon cycling (Ciais et
42 al., 2013; Dai et al., 2012; Raymond & Spencer, 2015). A large fraction of tDOC is remineralized
43 in ocean margin environments (Bélanger et al., 2006; Letscher et al., 2011; Painter et al., 2018).
44 For instance, it is reported that 40%–70% of tDOC is remineralized on the Louisiana Shelf, in the
45 Eurasian Arctic Shelf Sea and in the Sunda Shelf Sea before reaching the open ocean (Fichot &
46 Benner, 2014; Kaiser et al., 2017; Zhou et al., 2021). The remineralization results in the formation
47 of dissolved inorganic carbon (DIC) along with transformation of nutrient elements, thus causing
48 ocean acidification (Capelle et al., 2020; Semiletov et al., 2016; Wit et al., 2018; Zhou et al., 2021)

49 and influencing nutrient distributions (Alling et al., 2012; Qualls & Richardson, 2003; Vähätalo &
 50 Zepp, 2005). In addition, a fraction of tDOC—chromophoric dissolved organic matter (CDOM)
 51 can absorb light, causing light attenuation in natural waters and affecting primary productivity and
 52 other biological activities (Aksnes et al., 2009; Martin et al., 2021; Urtizberea et al., 2013).

53 Since terrestrial dissolved organic matter (tDOM) is rich in CDOM and fluorescent DOM
 54 (FDOM), absorbance and fluorescence spectroscopy are widely exploited to trace tDOC in aquatic
 55 environments, due to their high sensitivity and ease of measurement (Bauer & Bianchi, 2011;
 56 Coble, 2007; Dittmar, 2015; Stedmon & Nelson, 2015). The most commonly used optical
 57 properties (Table 1) include absorption coefficients (a_λ , m^{-1}), CDOM spectral slopes (such as
 58 $S_{275-295}$, nm^{-1}) and the CDOM spectral slope ratio ($S_R = S_{275-295}/S_{350-400}$), specific ultraviolet
 59 absorbance (SUVA_{254} , $\text{L mg-C}^{-1} \text{ m}^{-1}$), the fluorescence index (FI) and the humification index
 60 (HIX).

61

62 Table 1. Description of widely used optical properties indicating sources and compositions of DOM.

Optical property	Provided information	Reference
a_λ (m^{-1})	Represents CDOM concentration, often linearly correlated to DOC and lignin phenol concentrations in different aquatic environments	Fichot and Benner (2011); Hernes and Benner (2003); Osburn et al. (2016); Vantrepotte et al. (2015)
$S_{275-295}$ (nm^{-1})	Negatively correlated to DOM apparent molecular weight, exhibits exponential relationship with concentration of lignin phenols	Del Vecchio and Blough (2002); Fichot and Benner (2012); Helms et al. (2008)
S_R	Higher values indicate higher content of low apparent molecular weight components in DOM; increases upon photo exposure	Helms et al. (2008)
$S_{320-412}$ (nm^{-1})	An indicator of freshly produced autochthonous marine DOM, strong linear correlation to DOC-specific a_λ during phytoplankton bloom	Danhiez et al. (2017)
SUVA_{254} ($\text{L mg-C}^{-1} \text{ m}^{-1}$)	Shows linear relationship with aromaticity of DOM	Cartisano et al. (2018); Chin et al. (1994); Hur et al. (2006); Weishaar et al. (2003)
FI	DOM is likely to be terrestrial when $\text{FI} < 1.4$, while is more marine-sourced with higher FI	Cory et al. (2010); McKnight et al. (2001)
HIX	An indicator of content of humic substances or extent of humification in DOM, higher values corresponds to higher humification level	Ohno (2002)
BIX	An indicator of autochthonous biological activity, high values (>1) indicate dominance of aquatic DOM	Huguet et al. (2009)

63 Typically, tDOC is characterized by high values for a_λ , $SUVA_{254}$ and HIX, and low values for
64 $S_{275-295}$, S_R and FI (Gandois et al., 2014; Huguet et al., 2009; Kida et al., 2018; Stedmon et al.,
65 2011). In addition, parallel factor analysis (PARAFAC) of FDOM spectra is commonly used to
66 identify and quantify terrestrial fluorescent components to trace tDOC distribution in natural
67 environments (Murphy et al., 2008; Stedmon et al., 2003). Apart from these indices of terrestrial
68 source materials, the FDOM biological index (BIX) and more recently the CDOM spectral slope
69 between 320 and 412 nm ($S_{320-412}$, nm^{-1}) are used as tracers for in-situ production of autochthonous
70 DOM (Table 1).

71 However, while these optical properties are clearly useful, especially as qualitative markers for
72 identifying the presence and biogeochemical cycling of tDOC, it is still often unclear how accurate
73 they really are as tracers of total tDOC across coastal gradients where tDOC undergoes extensive
74 remineralization. Several studies have shown that some of the optical properties (a_λ , $S_{275-295}$) are
75 related to tDOC composition in estuarine and coastal environments, and that these optical
76 properties can therefore be used to quantify tDOC concentration (Fichot & Benner, 2012; Fichot
77 et al., 2016; Hernes & Benner, 2003). However, on the one hand, terrigenous CDOM and FDOM
78 may be more labile and lost preferentially relative to bulk tDOC, especially when subject to
79 photodegradation (Benner & Kaiser, 2011; Moran et al., 2000; Osburn et al., 2009). Yet on the
80 other hand, tDOC itself can only be estimated from proxy measures, and comparisons between
81 optical properties and tDOC have primarily relied on lignin phenols as a biomarker to quantify
82 tDOC. While lignin phenols unambiguously show that tDOC is present, they are only a small
83 fraction of the bulk tDOC (Fichot & Benner, 2012; Louchouart et al., 2000; Osburn & Stedmon,
84 2011), and may also decompose more easily than bulk tDOC during remineralization, especially
85 from photodegradation (Benner & Kaiser, 2011; Cao et al., 2018; Hernes & Benner, 2003). This
86 is further demonstrated by the fact that lignin phenols are scarce in the open-ocean DOC pool
87 (Hedges et al., 1997; Meyers-Schulte & Hedges, 1986; Opsahl & Benner, 1997), although
88 molecular and carbon isotope data suggest that oceanic DOC may in fact contain more tDOC than
89 previously recognised (Cao et al., 2018; Medeiros et al., 2016; Zigah et al., 2017). Moreover, few
90 studies have compared the various different optical properties comprehensively to evaluate which
91 are the most reliable for tracing tDOC in natural samples with mixed sources. Where systematic
92 comparisons have been conducted, they have been largely based on laboratory studies using DOM
93 from a limited range of plant, soil, or microbial sources, and subjected to purely photochemical or

94 purely microbial degradation experiments (Hansen et al., 2016; Lee et al., 2018). Specifically,
95 Hansen et al. (2016) showed that individual optical properties depended on both source and DOM
96 degradation process, with photochemical and microbial degradation often causing opposing
97 changes. They recommended that multiple optical properties should be used to evaluate DOM
98 sources in a qualitative perspective but did not show any quantitative information. Similarly, Lee
99 et al. (2018) concluded that SUVA, BIX and FI are most reliable as indicators of DOM source
100 because they are rarely affected by biogeochemical processes, but they did not derive statistical
101 relationships between optical properties and tDOC either. While these laboratory experiments have
102 provided important insights, we do not know how closely these results resemble what happens in
103 the coastal environment, where the DOM pool consists of many more different sources, and
104 physical, photochemical, and microbial processes interact in potentially complex ways (Antony et
105 al., 2018; Karen & Mary Ann, 1999; Miller & Moran, 1997). Consequently, more environmental
106 datasets are needed in which optical parameters can be directly compared and related to the actual
107 tDOC concentration across a known gradient of tDOC remineralization.

108 In this study, we used a multi-year time series of DOC concentration, DOC and DIC carbon stable
109 isotope composition, and DOM optical analysis from coastal Southeast Asia. Southeast Asia's
110 extensive tropical peatlands deliver around 10% of global land–ocean DOC flux (Baum et al.,
111 2007; Huang et al., 2017; Moore et al., 2011), while the region's archipelagic geography and
112 monsoon-driven ocean current reversal result in long water residence times on the shelf (Mayer et
113 al., 2022), allowing the majority of tDOC to be remineralized within the shelf sea (Wit et al., 2018;
114 Zhou et al., 2021). We used a carbon stable isotope mass balance approach to calculate both the
115 percentage contribution of tDOC to the bulk DOC pool (tDOC%) and the proportion of tDOC that
116 had been remineralized to DIC. This allows us to test how accurately different optical properties
117 can quantify tDOC%, and also to test whether any of the optical properties change purely as a
118 function of the extent of tDOC remineralization. In addition, we compared our environmental data
119 to results obtained from laboratory tDOC remineralization experiments to examine whether the
120 changes in optical properties during such simplified experiments reflect the patterns we observed
121 in our environmental data. This study not only provides a comprehensive dataset of a hotspot for
122 carbon cycling investigation to fill the gap in global coastal carbon and optical analysis, but also
123 proves the validity of applying spectroscopic techniques to broadly trace tDOC quantitatively in
124 natural environment.

125 **2 Dataset and Methods**

126 2.1 Datasets used in the present analysis

127 The main dataset used in the present analysis is a multi-year time series of DOC concentration,
128 stable carbon isotope composition, and optical properties collected in the Singapore Strait. In the
129 Singapore Strait, the monsoon system causes a seasonal reversal of water currents (Mayer et al.,
130 2022; Susanto et al., 2016; van Maren & Gerritsen, 2012): this causes tDOC originating from
131 peatlands on Sumatra to be transported to our study site during the Southwest (SW) Monsoon
132 (May to September), while water from the South China Sea with a mostly marine DOC pool is
133 delivered during the Northeast (NE) Monsoon (November to March) (Zhou et al., 2021). The map
134 of the study area is provided as Figure S1 in supporting information (SI). The present analysis
135 extends this time series by one more year compared to our previous publications (Zhou et al. 2021;
136 Martin et al. 2021), and focuses on comparing the performance of different optical properties in
137 tracing actual tDOC in coastal environment. While our previous publications only used part of the
138 optical dataset, mostly as supporting data to qualitatively confirm the monsoon-driven tDOC input,
139 the present study provides a comprehensive analysis to determine how the optical properties relate
140 quantitatively to variation in natural tDOC concentration and remineralization.

141 Because we lack optical data from the peatland-draining rivers on Sumatra that form the riverine
142 endmember for our study site (Martin et al., 2022; Zhou et al., 2021), we complement our analysis
143 using two other data sources. For CDOM absorption (as a_{440}), we calculated the discharge-
144 weighted average for the main peatland-draining rivers based on Wit et al. (2018) and Siegel et al.
145 (2019), detailed in Section 2.5.2. The resulting values of a_{440} and DOC follow the same CDOM-
146 DOC relationship found for the various peatland-draining rivers in Sarawak (Figure S2; Martin et
147 al., 2018). This indicates that the tDOC composition and optical properties are broadly similar
148 across Southeast Asian peatlands, which is also consistent with the fact that DOC concentrations
149 in peatland-draining rivers follow a single, strong relationship to catchment peatland cover across
150 both Sumatra and Borneo (Rixen et al., 2022). Therefore, for the other optical properties, we used
151 CDOM and FDOM data acquired from three expeditions in rivers in Sarawak, Borneo (Martin et
152 al., 2018; Zhou et al., 2019). The Sarawak data were divided into three categories: peat-majority

153 rivers (salinity <1), with catchment peatland coverage $\geq 50\%$, non-peat-majority rivers (salinity <1),
154 with catchment peatland coverage $<50\%$, and Sarawak estuarine and coastal water (salinity ≥ 1).

155 2.2 Singapore Strait timeseries sampling

156 The Singapore Strait timeseries data were collected from October 2017 to July 2021. Water
157 samples were collected from 5-m depth at two sites in the Singapore Strait using a Niskin bottle.
158 Sampling was undertaken monthly except during pandemic-related restrictions. The water was
159 filtered onboard through a pre-rinsed 0.22 μm polyethersulfone membrane (Supor, Merck
160 Millipore) with a peristaltic pump. All vials and tubes had been washed with 1 M HCl and ultrapure
161 water (18.2 $\text{M}\Omega\text{ cm}^{-1}$). Amber borosilicate vials for DOC and optical measurements were pre-
162 combusted at 450 $^{\circ}\text{C}$ for 4 h after washing. At each station, a depth profile of salinity and
163 temperature was measured using a fastCTD Profiler (Valeport Ltd). The water column typically
164 does not show stratification (Martin et al., 2022).

165 2.3 Sample analysis

166 2.3.1 Dissolved carbon and total alkalinity analysis

167 Triplicate DOC samples were acidified with 50% sulfuric acid, stored at +4 $^{\circ}\text{C}$, and analysed on a
168 Shimadzu TOC-L system with a high-salt combustion kit. For each sample, 5–7 replicate injections
169 were performed to ensure that the coefficient of variation was less than 2%. Deep-sea water (42–45
170 $\mu\text{mol/L}$ DOC) from the University of Miami, USA was analysed on each run (long-term mean and
171 standard deviation from 2017–2022: $46.7 \pm 4.2\ \mu\text{mol/L}$).

172 Dissolved inorganic carbon (DIC) was analysed on an Apollo SciTech AS-C5 DIC analyser at
173 room temperature ($22 \pm 0.5^{\circ}\text{C}$). Each sample was measured 3–5 times to obtain a relative standard
174 deviation less than 0.1%. Certified reference material (CRM) from Scripps Institution of
175 Oceanography (Batch 172) or an in-house secondary standard of Singapore Strait seawater was
176 used for calibration. The analytical precision was $\pm 0.15\%$.

177 Total alkalinity (TA) was analysed at room temperature ($22 \pm 0.5^{\circ}\text{C}$) on an Apollo SciTech AS-
178 ALK2 titrator with a ROSS combination glass pH electrode (Orion 8302BNUMD), conducting
179 the Gran titration (Gran, 1952) automatically. The titration was conducted with a 25-mL aliquot

180 and 0.1 M hydrochloric acid (HCl) and repeated 2–4 times for each sample. The CRM or secondary
181 standard above was used for calibration and the analytical precision was $\pm 0.13\%$.

182 Stable isotope ratio of DOC ($\delta^{13}\text{C}_{\text{DOC}}$) samples were stored at $-20\text{ }^{\circ}\text{C}$, then thawed and acidified
183 with 35 μL concentrated HCl to pH of 2–3 and analyzed at the Ján Veizer Stable Isotope
184 Laboratory, University of Ottawa, Canada (2-sigma analytical precision of $\pm 0.4\%$).

185 Stable isotope composition of DIC ($\delta^{13}\text{C}_{\text{DIC}}$) samples were partly analyzed at the Stable Isotope
186 Facility, University of California, Davis using a GasBench II system with a Thermo Scientific
187 Delta V Plus isotope-ratio mass spectrometer (analytical precision of $\pm 0.1\%$), and partly analysed
188 in the Marine Geochemistry Laboratory, Nanyang Technological University, Singapore as
189 described previously (Zhou et al., 2021), with analytical precision of $\pm 0.2\%$.

190 2.3.2 Optical analyses

191 Samples for CDOM and FDOM were analysed at room temperature ($\sim 22\text{ }^{\circ}\text{C}$) on the day of
192 collection or after overnight storage at $+4\text{ }^{\circ}\text{C}$. CDOM absorption was measured on a Thermo
193 Evolution 300 dual-beam spectrophotometer from 230 nm to 900 nm at 1-nm resolution in 10-cm
194 or 2-mm quartz cuvettes with ultrapure water as a reference. They were baseline-corrected and
195 analysed using the R package “hyperSpec” (Beleites & Sergo, 2018; Green & Blough, 1994). We
196 calculated the following properties: a_{350} or a_{440} (m^{-1} ; Green and Blough, 1994), $S_{275-295}$ (nm^{-1} ;
197 Helms et al., 2008), $S_{320-412}$ (nm^{-1} ; Danhiez et al., 2017), S_{R} (Helms et al., 2008) and SUVA_{254} (L
198 $\text{mg-C}^{-1}\text{ m}^{-1}$; Weishaar et al., 2003).

199 FDOM steady-state fluorescence excitation–emission matrices (EEMs) were measured on a
200 HORIBA Jobin Yvon FluoroMax-4 fluorometer in a 1-cm or 3-mm quartz cuvette at excitation
201 wavelength of 250–450 nm with 5-nm intervals and emission wavelength of 290–550 nm with 2-
202 nm intervals, with 5 nm for both bandwidths. EEMs of ultrapure water were analyzed to record
203 Raman and Rayleigh scattering. EEMs were processed using the Matlab drEEM toolbox (Murphy
204 et al., 2013) to achieve inner filter effects (IFE) correction, blank subtraction, and conversion to
205 Raman units (RU; Lawaetz & Stedmon, 2009). We calculated the fluorescence index (FI; Cory et
206 al., 2010), humification index (HIX; Ohno, 2002) and biological freshness index (BIX; Huguet et

207 al., 2009). The calculations of these optical properties and the information that they are considered
208 to provide are described in Table 1.

209 2.4 Photodegradation experiments

210 We used data from the same photodegradation experiments reported by Zhou et al. (2021) that
211 were conducted with water samples from a peatland-draining river on Borneo (Maludam River)
212 and from the Singapore Strait during the SW Monsoon. Although we used the same dataset as the
213 previous publication, our purpose here is to identify whether any of the properties is quantitatively
214 related to the extent of tDOC photochemical remineralization, which was not addressed in Zhou
215 et al. (2021). The experimental methods are described in detail in Zhou et al. (2021); briefly, 30
216 mL filtered water was added into replicate cylindrical quartz cells (50 mm pathlength, 50 mm
217 diameter) with Teflon screw caps, and irradiated under a xenon lamp with daylight optical filter in
218 an Atlas Suntest CPS + solar simulator. Dark controls of filtered water were placed in Duran bottles
219 fully wrapped with aluminium foil in the solar simulator. Two replicates each for light-exposed
220 and control samples were withdrawn at each time point for DOC concentration and optical
221 measurements.

222 2.5 Statistical analysis

223 2.5.1 Parallel factor analysis

224 Parallel factor analysis (PARAFAC) can partition fluorescence EEMs into underlying fluorescent
225 components to characterize and quantify the relative contribution of different fractions (Cory &
226 McKnight, 2005; Murphy et al., 2013; Stedmon & Bro, 2008). A total of 550 sample EEMs,
227 including environmental data from the Singapore Strait and Sarawak, Borneo, and experimental
228 data from photodegradation and bio-incubation for coastal seawater and Maludam water (Zhou et
229 al., 2021; Zhou et al., 2019), were analysed by PARAFAC using the drEEM toolbox in MATLAB
230 (Murphy et al., 2013). Eleven EEMs were excluded because they were identified as outliers by
231 visual inspection. A five-component model was generated and validated by split-half analysis. The
232 excitation and emission peak wavelengths of the 5 components (C1–C5) were compared with other
233 studies (Coble, 1996; Murphy et al., 2008; Osburn et al., 2016; Stedmon & Markager, 2005a;
234 Stedmon et al., 2003; Zhou et al., 2019) to attribute possible sources of the DOM fractions they
235 represent (Figure S3 and Table S1). The fluorescence intensity at the excitation and emission

236 maximum (F_{max}) is a measure of the contribution to total fluorescence and of the concentration
237 of each DOM fraction represented by the corresponding PARAFAC component.

238 2.5.2 Mixing models and carbon isotope mass balance calculation

239 We assessed the mixing behaviour of the optical parameters across the whole salinity gradient.
240 Moreover, we used a carbon isotope mass balance approach to calculate the amount of tDOC that
241 has been remineralized, following the approach of previous publications (Humborg et al., 2017;
242 Samanta et al., 2015; Su et al., 2017; Zhou et al., 2021). Specifically, we used two-endmember
243 mixing models to estimate expected distributions of measured parameters across the salinity
244 gradient for purely conservative mixing between a riverine and a marine endmember. We obtained
245 riverine endmember values of DOC concentration, a_{440} , $\delta^{13}\text{C}_{\text{DOC}}$, $\delta^{13}\text{C}_{\text{DIC}}$, DIC and TA (Table S2)
246 by taking discharge-weighted averages of data from the four main peat-draining rivers on Sumatra
247 (the Indragiri, Kampar, Siak and Batanghari in Figure S1b) that are the most plausible sources of
248 peatland tDOC to the Singapore Strait (Siegel et al., 2019; Siegel et al., 2009; Wit et al., 2018;
249 Zhou et al., 2021). The resulting riverine endmember values were corroborated by the fact that the
250 a_{440} and DOC fall onto the same CDOM–DOC relationship found for the various peatland-draining
251 rivers in Sarawak (Figure S2; Martin et al., 2018). This suggests that peatland tDOM pools and
252 their optical properties are quite similar across Southeast Asian peatlands, and that variation in
253 tDOC concentration among rivers is primarily a function of catchment peatland coverage rather
254 than reflecting differences in tDOM characteristics (Rixen et al., 2022). Since $\delta^{13}\text{C}_{\text{DOC}}$ in peatland-
255 draining rivers of Southeast Asia mostly ranges between -30 and -28‰ (Evans et al., 2014;
256 Gandois et al., 2014; Zhu et al., 2020), we adopted an approximated value of -29‰ as the riverine
257 endmember. Photodegradation and combined photo-biodegradation of tDOC can cause
258 fractionation of -1.4‰ to -5.8‰ between the original $\delta^{13}\text{C}_{\text{DOC}}$ and the produced $\delta^{13}\text{C}_{\text{DIC}}$ values
259 (Opsahl & Zepp, 2001; Osburn et al., 2001; Spencer, Stubbins, et al., 2009). Given that peatland-
260 derived tDOC in Southeast Asia appears to be fairly refractory to direct biodegradation but shows
261 high photo-lability (Nichols & Martin, 2021; Zhou et al., 2021), we adopted a fractionation of
262 -3‰ , thus taking -32‰ as the $\delta^{13}\text{C}_{\text{DIC}}$ value for remineralized tDOC in our calculation. Marine
263 endmember values were determined as averages of the measurements during late February and
264 March, when marine water from the open South China Sea predominates in the Singapore Strait

265 with little tDOC presence (Figure 1). The fractional contributions of freshwater and seawater were
266 determined from salinity.

267 To quantify the remaining tDOC concentration and how much tDOC had already been
268 remineralized to DIC, we assumed that tDOC is the only source of remineralized terrigenous
269 carbon while terrigenous POC does not make contribution, and that autochthonous DOC cycling
270 does not influence our estimation. These assumptions are discussed in Section 4.1. The equations
271 for the carbon isotope mass balance calculation are provided in the SI (Samanta et al., 2015; Zhou
272 et al., 2021). Briefly, the concentration of tDOC in each sample was calculated from the measured
273 $\delta^{13}\text{C}_{\text{DOC}}$ and DOC concentration using a two-endmember isotope mixing model. We refer to this
274 as “remaining tDOC concentration” because it represents the fraction of the initial tDOC input that
275 remains in form of DOC, as opposed to the fraction that has been remineralized. Based on the
276 known stoichiometric effects of primary production, remineralization, calcium carbonate
277 production and dissolution, and air-sea CO_2 exchange on the deviations of DIC and TA from their
278 conservative mixing values (Zeebe & Wolf-Gladrow, 2001), and on the fractionation of $\delta^{13}\text{C}$
279 (Opsahl & Zepp, 2001; Osburn et al., 2001; Spencer, Aiken, et al., 2009), the amount of tDOC in
280 a sample that has already been remineralized can be back-calculated as in other studies (Humborg
281 et al., 2017; Samanta et al., 2015; Su et al., 2017; Zhou et al., 2021). We refer to the sum of
282 remaining tDOC and remineralized tDOC as the “total initial tDOC concentration”.

283 The mixing patterns of both the remaining tDOC and total initial tDOC closely resembled
284 conservative mixing, suggesting that physical mixing still dominates the concentration changes in
285 our sampling site and that the difference between remaining tDOC and total initial tDOC results
286 mainly from remineralization upstream of our site. As such, using our conservative mixing model,
287 we estimated the apparent (and actual) riverine endmember DOC concentration by extrapolating
288 the remaining tDOC (and total initial tDOC) back to salinity 0. The errors of tDOC extrapolation
289 were the standard deviations calculated from Monte Carlo simulation by taking all uncertainties
290 of measurements and calculation into consideration (Table S2) and recalculating 10,000 times.
291 Similarly, the apparent riverine endmember value of a_{440} was obtained by extrapolating our a_{440}
292 timeseries data to salinity 0 based on the conservative mixing model. The actual riverine
293 endmember a_{440} was obtained from the discharge-weighted average as explained in the previous
294 paragraph. The errors of apparent and actual riverine endmember a_{440} were obtained directly from

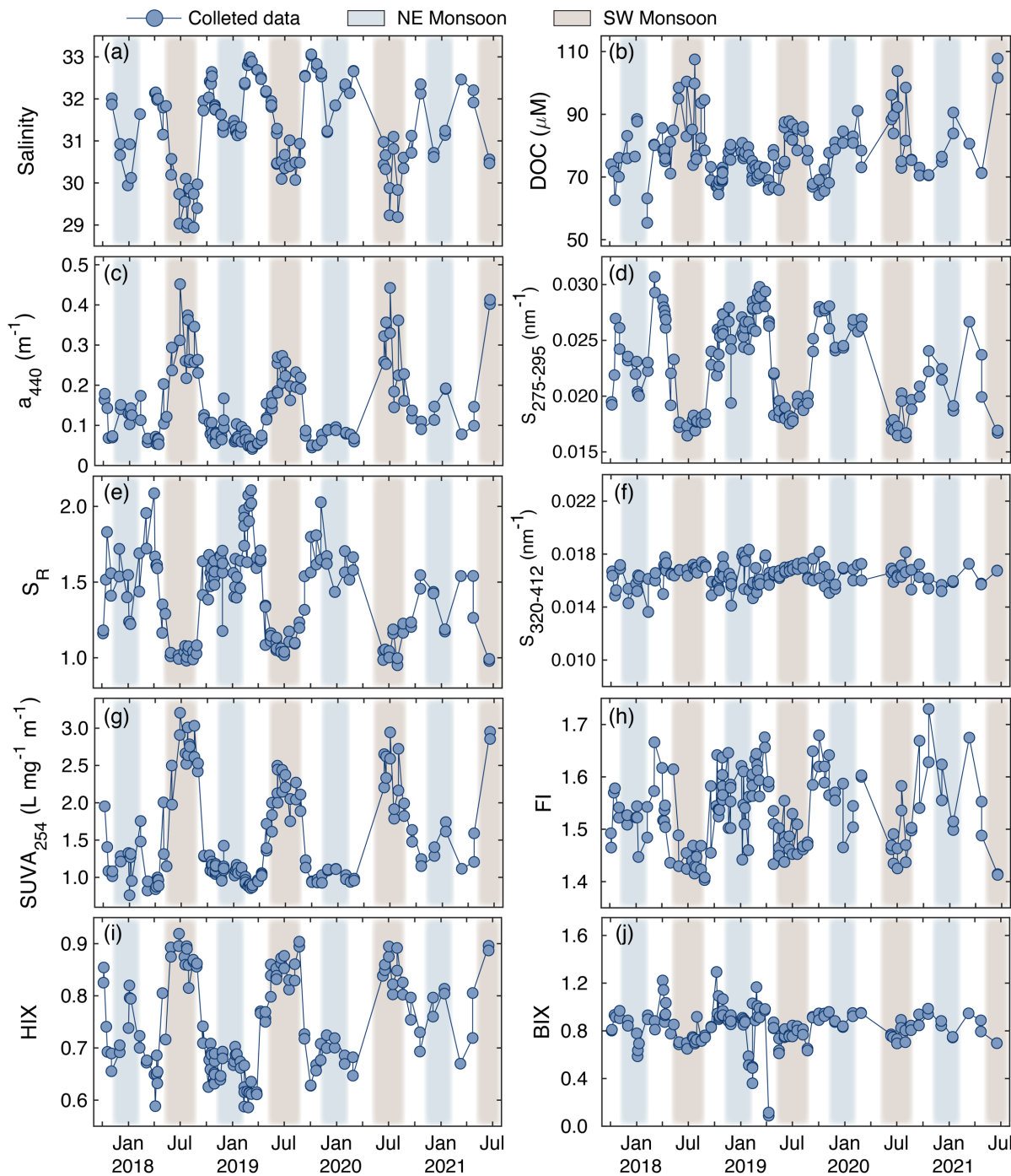
295 the linear regression of a_{440} against salinity and as the standard deviation from the discharge-
296 weighted average calculation, respectively. These riverine endmember values are presented in
297 Table S3.

298 **3 Results**

299 3.1 Temporal variation of DOM optical properties in the Singapore Strait

300 There is a seasonal change in biogeochemistry in the Singapore Strait driven by the monsoonal
301 current reversal. The extended timeseries data in the present study demonstrates similar seasonal
302 patterns compared to our previous publications (Martin et al., 2022; Martin et al., 2021; Zhou et
303 al., 2021). Here, we further examine additional optical parameters ($S_{320-412}$, FI, BIX, HIX, and C2
304 from PARAFAC analysis) to examine the application of spectroscopic techniques to quantify the
305 concentration and remineralization of tDOC in natural environment directly, instead of using other
306 proxies such as lignin phenols to represent the bulk tDOC.

307 During the SW Monsoon (May to September), currents carry freshwater from the east coast of
308 Sumatra to our study site in the Singapore Strait, causing salinity to drop from approximately 33
309 to around 29 (Figure 1a and Figure S1a). DOC concentrations and CDOM (a_{440}) increased by,
310 respectively, 1.2–1.7 and 2–10 times compared to other seasons, with maximum concentrations
311 showing clear interannual variability (Figure 1b–c). $S_{275-295}$ and S_R showed the lowest values
312 during the SW Monsoon, in the range of 0.016–0.020 nm^{-1} and 0.95–1.23, respectively (Figure
313 1d–e). In contrast, $SUVA_{254}$ and HIX reached peak values of higher than 3.3 $\text{L mg-C}^{-1} \text{m}^{-1}$ and
314 0.9, respectively (Figure 1f–g). This seasonality in the optical properties indicates a large amount
315 of tDOC input by freshwater. During the NE Monsoon and the following early inter-monsoon
316 season (December to March), water without much terrestrial input flows from the South China Sea
317 to the study site, resulting in relatively high $S_{275-295}$, low S_R , low $SUVA_{254}$ and low HIX. In
318 contrast, FI and BIX tended to have consistently low values during the SW Monsoon, respectively
319 at around 1.4 and 0.7, but exhibited variable values in the other seasons, so that the overall seasonal
320 contrast was less strong than that for optical properties typically associated with tDOC (Figure
321 1h–i). Finally, $S_{320-412}$ showed very little variation and no seasonality, with values mostly from
322 0.015 to 0.019 nm^{-1} (Figure 1j).



323
 324 Figure 1. Timeseries data of salinity, DOC concentration and optical properties in the Singapore Strait. Data from
 325 Northeast (NE) Monsoon and Southwest (SW) Monsoon are distinguished by different shading colors. Salinity, DOC

326 concentration, a_{440} , $S_{275-295}$, S_R , $SUVA_{254}$, FI and HIX presented seasonal changes driven by the monsoonal current
327 reversal, while $S_{320-412}$ and BIX showed limited or no seasonality.

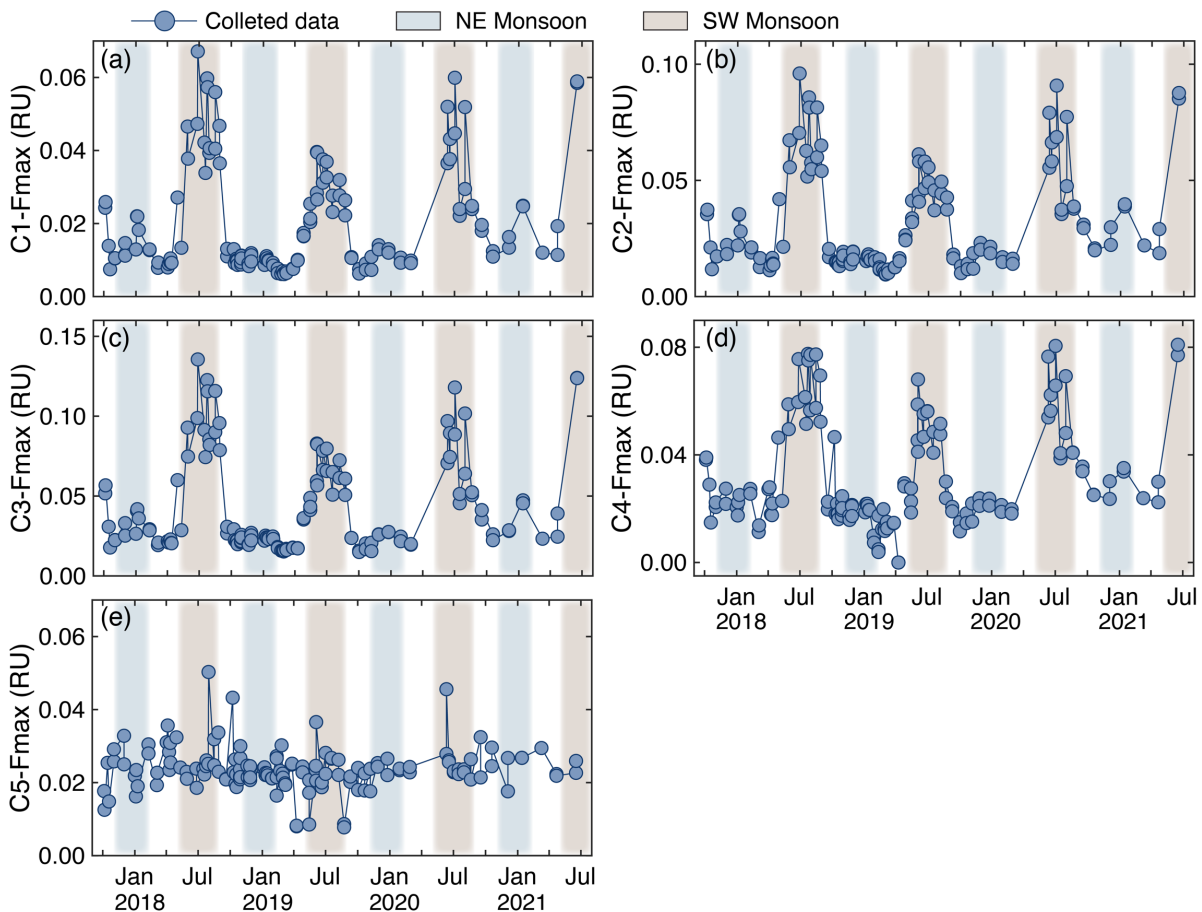
328

329 3.2 Temporal variation of PARAFAC components in the Singapore Strait

330 Five fluorescent components (C1–C5) were identified by PARAFAC analysis (Figure S3 and
331 Table S1), explaining 99.4% of the variability of the dataset. Among these 5 components, C1, C2
332 and C3 emitted mostly at visible wavelengths, which may suggest a large contribution of molecular
333 conjugation or interaction (Chen et al., 2020; Coble, 1996; Del Vecchio & Blough, 2004a).
334 Specifically, C1 has been identified in different water bodies (Stedmon & Markager, 2005a) and
335 is typically associated with fulvic acid fluorophores. Emission peaks of C2 at around 430 nm with
336 two excitation maxima at 250 nm and 430 nm have been respectively assigned as humic-like
337 components peak A and C in previous work (Coble, 1996), and have been widely thought to
338 represent DOM fractions with high apparent molecular weight (Jaffé et al., 2014; McKnight et al.,
339 2001; Stedmon et al., 2003; Yamashita et al., 2008). C2 has been reported to be highly correlated
340 with lignin phenol concentration (Yamashita et al., 2015) and is found only at low intensities in
341 the open ocean (Murphy et al., 2008), thus is considered to be terrestrial derived. DOC-normalized
342 C2 intensity was used previously to estimate tDOC percent contribution in the Sarawak FDOM
343 dataset (Zhou et al., 2019). C3 also resembled the maxima characteristic of peak A but possessed
344 a wider emission wavelength range, which has been found to be dominated by DOM derived from
345 forest and wetland regions (Stedmon et al., 2003). Although C4 was traditionally considered
346 related to marine humic-like material (Coble, 1996; Yamashita et al., 2015), it was related to
347 microbial processed materials (Grunert et al., 2021; Osburn et al., 2016) and was found to have
348 significant terrestrial signals in Southeast Asia (Harun et al., 2016; Zhou et al., 2019). In the present
349 study, the terrestrial origin of C4 was proven by the consistent seasonal change with freshwater
350 input caused by monsoon-driven currents. Finally, C5 showed high similarity to peak T and peak
351 B, which are considered as protein-like fluorophores produced from microbial processes, and
352 usually associated with fresh phytoplankton-produced DOM (Coble, 1996; Kowalczyk et al.,
353 2013; Stedmon & Markager, 2005b; Yamashita & Tanoue, 2003; Yang & Hur, 2014).

354 Generally, the signals of C1–C4 exhibited similar seasonal changes during the 4 years, with high
355 fluorescence contribution during the SW Monsoon, roughly 4–11 times greater than those during

356 other seasons (Figure 2a–d). This seasonality is consistent with the reported attribution of
 357 PARAFAC components mentioned above and the monsoon-driven freshwater delivery to the
 358 sampling site. There was also an interannual variability of peak values, consistent with that
 359 observed in DOC concentration, a_{440} and $SUVA_{254}$. Among these four components, their intensities
 360 followed an order of $C3 > C2 > C4 > C1$. In contrast, Fmax of C5 stayed within the range of
 361 0.015–0.035 RU without obvious seasonality (Figure 2e). This suggests that there is a baseline of
 362 marine-sourced DOM in the Singapore Strait that is hardly influenced by seasonal water advection
 363 and mixing.



364
 365 Figure 2. Timeseries data of FDOM component intensities derived from PARAFAC analysis. Components 1-4 were
 366 identified as terrestrial components as their variability was consistent with seasonal freshwater input. The highest

367 values were observed in SW Monsoon when tDOM is delivered from the west coast of Sumatra by water currents.
368 Component 5, which was attributed to marine-sourced DOM, showed little variability.

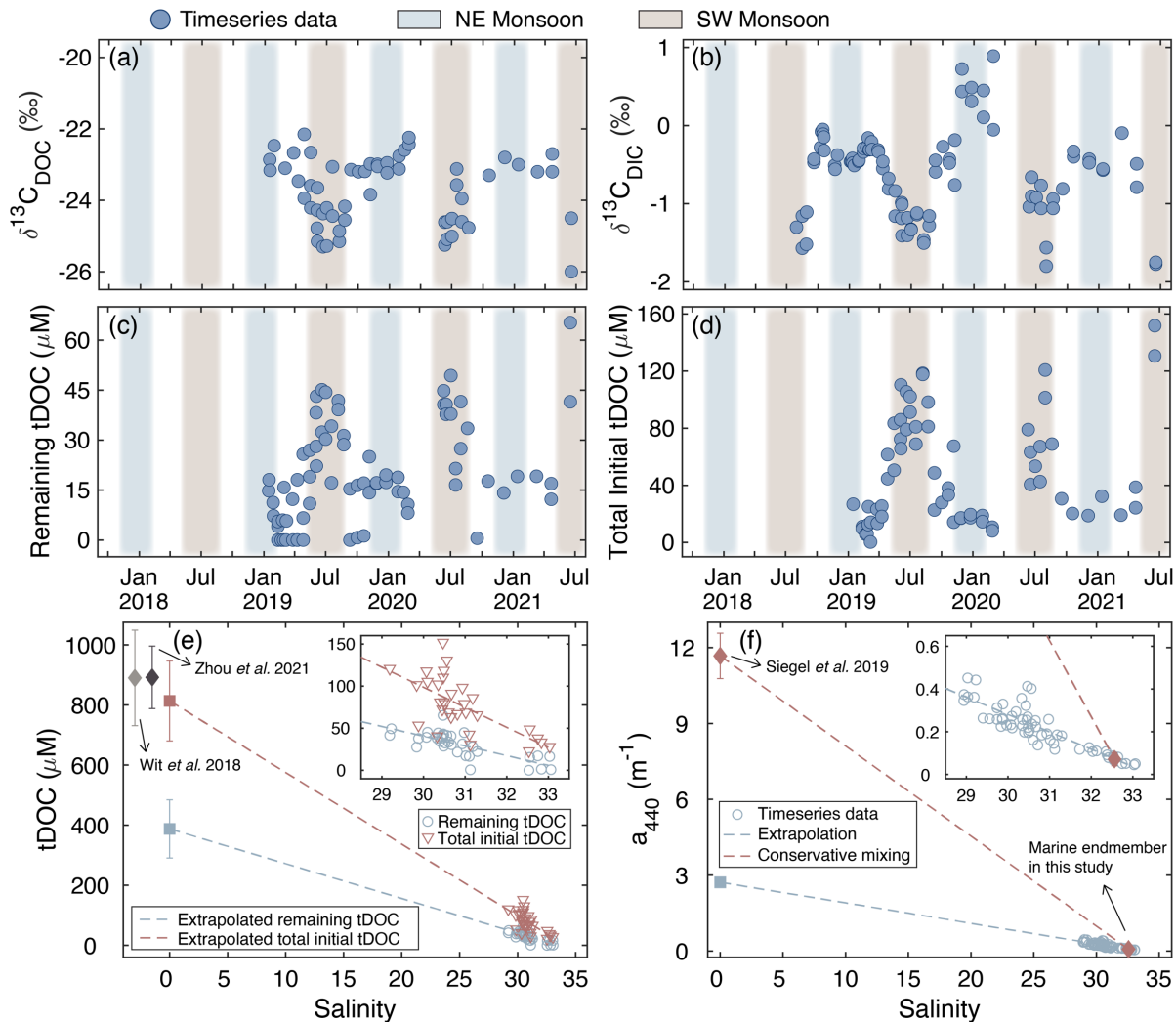
369

370 3.3 Carbon isotope mass balance and preferential CDOM loss relative to tDOC

371 During the SW Monsoon, $\delta^{13}\text{C}$ tended to be more negative for both the DOC and DIC pool, with
372 values mostly from -25.5‰ to -24‰ and -1.8‰ to -0.9‰ , respectively (Figure 3a–b), indicating
373 the large contribution of terrigenous carbon. Based on our carbon isotope mass balance, the
374 remaining tDOC and total initial tDOC concentrations reached peak values of $50\text{--}60\ \mu\text{M}$ and ~ 120
375 μM , respectively (Figure 3c–d). During the NE Monsoon and the following inter-monsoon
376 seasons, in contrast, the timeseries data exhibited the most enriched $\delta^{13}\text{C}_{\text{DIC}}$ and $\delta^{13}\text{C}_{\text{DOC}}$ and the
377 lowest values for the remaining tDOC and total initial tDOC concentrations.

378 Apparent conservative mixing was observed for both tDOC concentrations and CDOM absorption
379 (a_{440}) in the Singapore Strait (Figure 3e–f). By calculating linear regressions against salinity for
380 both remaining tDOC and total initial tDOC, we infer an apparent riverine tDOC concentration of
381 $389\pm 97\ \mu\text{mol L}^{-1}$ and an actual riverine tDOC concentration of $814\pm 133\ \mu\text{mol L}^{-1}$. Our actual
382 riverine tDOC concentration is within the uncertainty range of the discharge-weighted average
383 DOC ($890 \pm 159\ \mu\text{mol L}^{-1}$) reported from the four main peat-draining rivers in Sumatra that
384 represent the most plausible source of tDOC input to Singapore (Wit et al., 2018). Our estimate is
385 also very close (within 9%) to the value published previously based on a shorter timeseries (Zhou
386 et al., 2021). The difference between the apparent and actual endmember tDOC concentrations
387 indicates that, on average, 56% of the initial tDOC is remineralized before reaching our sampling
388 site.

389 We quantified CDOM using the a_{440} rather than a_{350} to allow a direct comparison to the data
390 published from Sumatra (Siegel et al., 2019; Siegel et al., 2009). CDOM absorption showed a
391 strong linear correlation with salinity in the Singapore Strait ($r^2 = 0.76$, $p < 0.01$, Figure 3f), from
392 which we infer an apparent riverine endmember a_{440} of $2.7\ \text{m}^{-1}$. This is 77% lower than the
393 discharge-weighted riverine endmember a_{440} of $11.7\ \text{m}^{-1}$ that we calculated based on the data in
394 Siegel et al. (2019) and Wit et al. (2018). We therefore conclude that on average 77% of CDOM
395 absorption is lost before reaching our sampling site. This shows that there is preferential loss of
396 CDOM relative to tDOC, albeit not by a very large amount.



397
 398 Figure 3. Timeseries data of stable carbon isotope ratios and tDOC concentrations, and mixing behaviours of tDOC
 399 and CDOM. (a) $\delta^{13}\text{C}_{\text{DOC}}$ and (b) $\delta^{13}\text{C}_{\text{DIC}}$ presented the most depleted values during the SW Monsoon due to freshwater
 400 input, while (c) the remaining tDOC and (d) total initial tDOC concentrations showed the highest values during this
 401 season. (e) The results of conservative mixing for tDOC concentrations suggested that on average 56% of tDOC is
 402 remineralized, while (f) on average 77% of CDOM is bleached before reaching our study site, showing some
 403 preferential removal of CDOM.

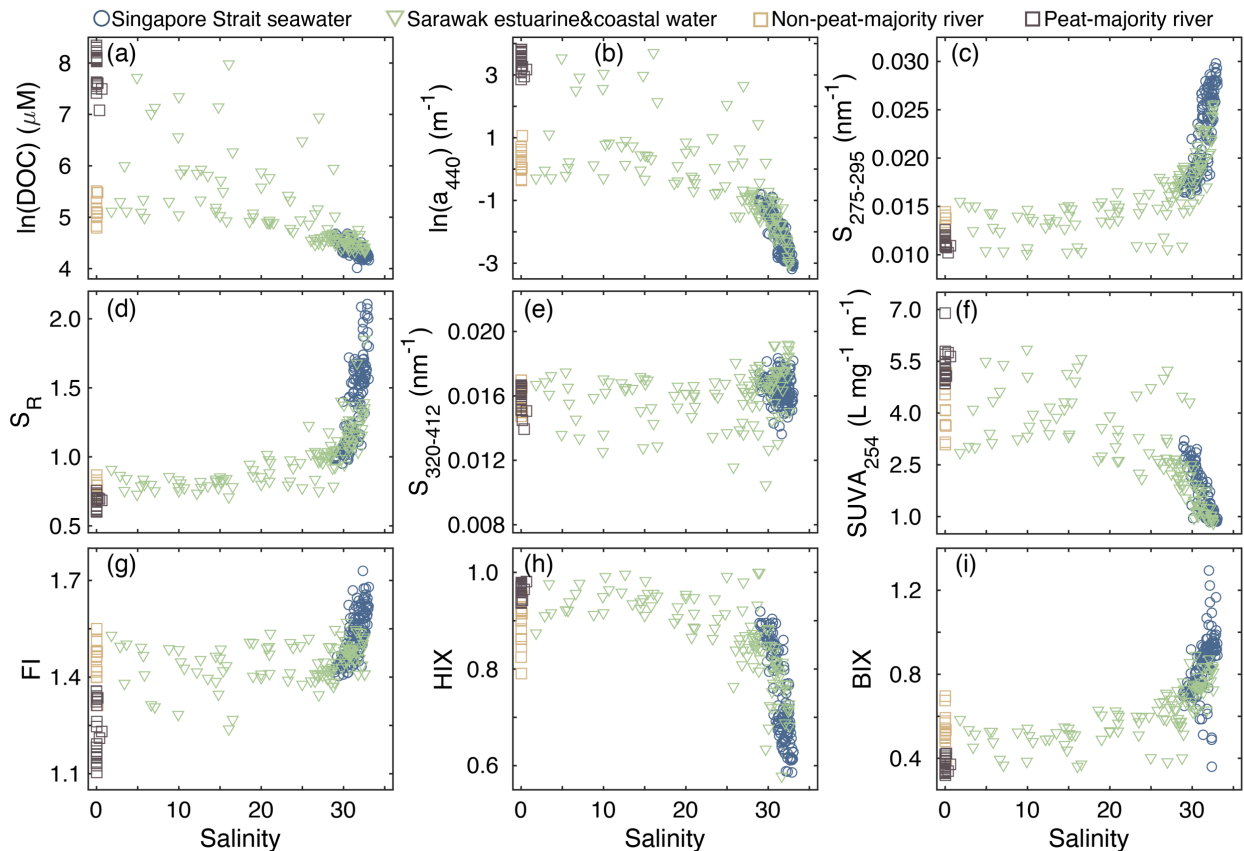
404

405 3.4 Mixing pattern of DOM optical properties in Singapore and Sarawak

406 The compiled Singapore and Sarawak carbon and optical data against salinity showed that the
 407 DOM properties at the two sites broadly fell within an overlapping range on the same mixing
 408 continuum (Figure 4). The Sarawak data showed a clear distinction for DOC concentration and for
 409 a_{440} of samples from rivers with >50% and <50% peatland in their catchments (squares in Figure

410 4). Clear differences between peat-majority and non-peat-majority rivers were also seen for
411 SUVA₂₅₄, FI, HIX, and BIX, but less so for the CDOM spectral slope parameters. At low salinities
412 (<25), corresponding to estuarine samples, high variability for DOC concentration, a_{440} and
413 SUVA₂₅₄ was observed while the values for $S_{275-295}$, S_R , FI, HIX and BIX were more compacted
414 (triangles in Figure 4).

415 Between salinities of 27–33, corresponding to more mixed coastal waters beyond the dominant
416 influence of a single river, the values of these DOM properties for Singapore and Sarawak coastal
417 water largely overlapped for a given salinity (triangles and circles in Figure 4). Given that the
418 marine endmember water for Singapore and Sarawak is the southern South China Sea, the overlap
419 in DOM properties for a given salinity suggests that the riverine endmembers from Sarawak and
420 Sumatra have similar average tDOM composition and optical properties, as also suggested by the
421 similar relationship of CDOM a_{440} to DOC concentration for the river data (Figure S2). Because
422 optical properties other than a_{440} have not been measured in rivers on Sumatra, we therefore use
423 the freshwater data from the river systems in Sarawak to provide indicative ranges of these
424 parameters for samples of pure tDOC in our further analysis of the Singapore data below.



425
 426 Figure 4. DOC and optical properties of coastal water in the Singapore Strait, and of rivers and estuarine/coastal waters
 427 in Sarawak (Borneo) against salinity. River data from Sarawak are distinguished by whether the catchment has >50%
 428 or <50% peatland. For all parameters, the data from the Singapore Strait fall within the same mixing continuum as
 429 coastal waters from Sarawak.

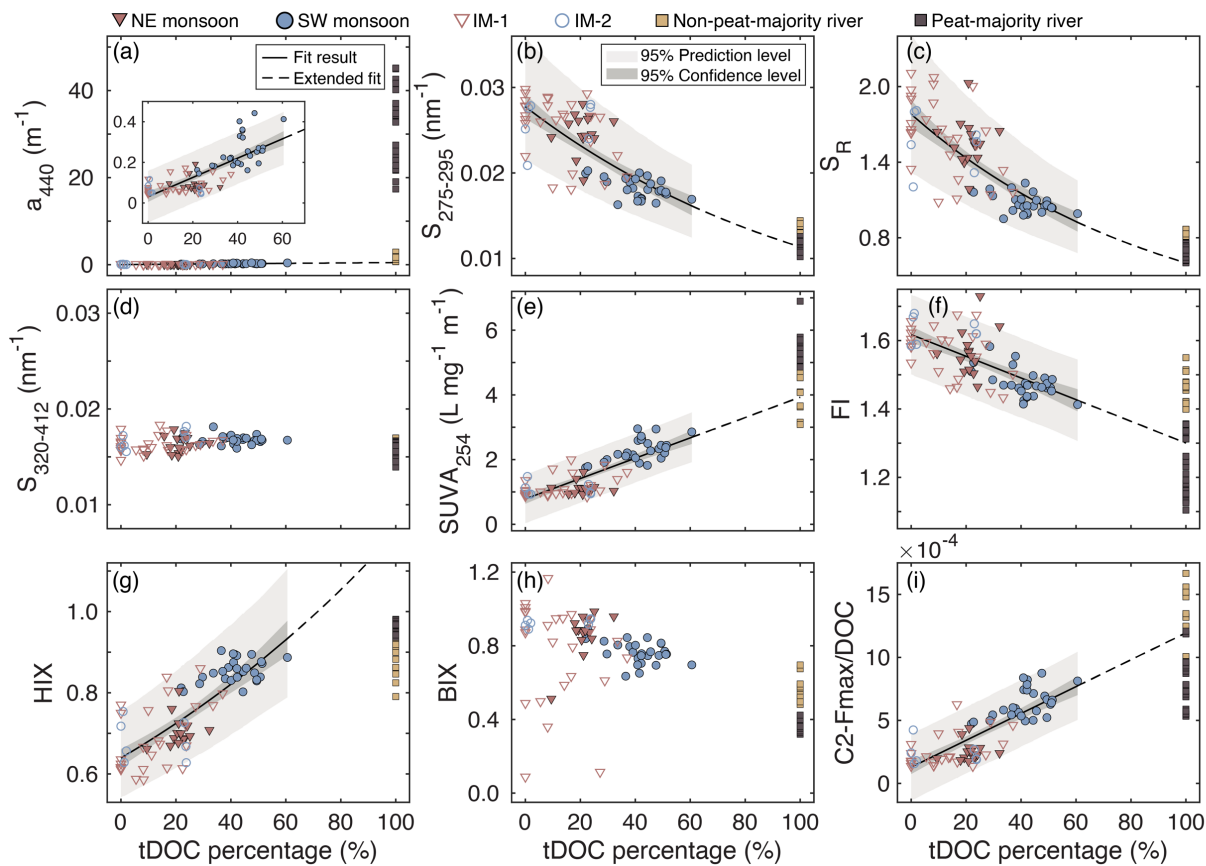
430

431 3.5 Relationships of optical properties to tDOC content

432 Our isotope mass balance calculation for the Singapore Strait timeseries allows us to estimate for
 433 each sample both the proportion of the bulk DOC pool that is tDOC and the amount of initially
 434 present tDOC that has been remineralized. We can therefore test how well the different optical
 435 properties are related to the tDOC content and whether they reflect the extent of prior
 436 remineralization. Given the similarity in DOM optical properties between our Singapore and
 437 Sarawak coastal water data (Figure 4 and Figure S2), we use the river data from Sarawak (at
 438 salinity 0) to provide an estimated range of values for the optical properties at 100% tDOC, prior

439 to experiencing remineralization in the coastal environment. The observed percentage of tDOC in
440 coastal water is the combined result of both water mass mixing and remineralization.

441 Most of the optical properties showed significant relationships with the percentage of bulk DOC
442 contributed by the remaining tDOC (tDOC%, Figure 5, statistical parameters are listed in Table
443 2). Specifically, a_{440} presented a strong and linear relationship with tDOC% (Figure 5a), although
444 owing to the preferential CDOM loss (Figure 3e–f) this relationship deviated from the river data.
445 The spectral slope properties $S_{275-295}$ and S_R showed exponential relationships with tDOC%, with
446 both r^2 being 0.55. When the relationships were extrapolated to 100% tDOC they fell in the range
447 of the Sarawak river data (Figure 5b–c), suggesting that these properties are applicable across the
448 full range of tDOC%. The CDOM spectral slope $S_{320-412}$, which is indicative of fresh primary
449 production of DOM (Danhiez et al., 2017), did not vary much throughout the whole tDOC% range
450 (Figure 5d). $SUVA_{254}$ was linearly related to tDOC% and had the highest r^2 (0.66) of any of the
451 optical properties (Figure 5e). Moreover, the relationship also fell within the range of the river data
452 when extrapolated to 100% tDOC. Furthermore, compared to $S_{275-295}$ and S_R , $SUVA_{254}$ showed
453 less scatter around the linear fitting line and possessed relatively narrower confidence and
454 prediction intervals. For the fluorescence properties, there was a linear relationship between FI and
455 tDOC% (Figure 5f) and the extrapolation fell within the range of collected river data, although the
456 river values showed relatively large scatter. In contrast, HIX showed an exponential relationship
457 with tDOC% and the relationship did not extrapolate into the range of the river data (Figure 5g).
458 There was no relationship of BIX against tDOC% because BIX, like $S_{320-412}$, is more related to
459 autochthonous marine DOM (Huguet et al., 2009). Finally, the DOC-normalized F_{max} value of
460 PARAFAC component 2 (C2- F_{max}/DOC), which was previously used to estimate tDOC
461 contribution in Sarawak estuaries (Zhou et al., 2019), was linearly related to tDOC%, showing
462 similarly high r^2 (0.64) as $SUVA_{254}$ and exhibiting good consistency with the river data (Figure
463 5i).



464
 465 Figure 5. Relationships between optical properties and percentage contribution of tDOC to total DOC (tDOC%). The
 466 relationships were calculated only with the Singapore Strait data during NE Monsoon, Inter-Monsoon-1 (IM-1, the
 467 intermonsoon after NE Monsoon), SW Monsoon and Inter-Monsoon-2 (IM-2, the intermonsoon after SW Monsoon),
 468 but were extrapolated to 100% tDOC to compare to the reference river data from Sarawak.

469

470 Table 2. Summary of statistical relationships of optical properties with tDOC% (all N=76, $p < 0.05$).

Optical property	Fitting formula	Parameter		Adjusted r^2	Consistent with river data*
		a	b		
a_{440} (m^{-1})	$y = a \times tDOC\% + b$	4.75×10^{-3}	3.08×10^{-2}	0.60	×
$S_{275-295}$ (nm^{-1})	$y = \exp(a \times tDOC\% + b)$	-8.52×10^{-3}	-3.59	0.55	√
S_R	$y = \exp(a \times tDOC\% + b)$	-1.06×10^{-2}	5.83×10^{-1}	0.55	√
SUVA ₂₅₄ ($L\ mg^{-1}\ C^{-1}\ m^{-1}$)	$y = a \times tDOC\% + b$	3.14×10^{-2}	7.86×10^{-1}	0.66	√
FI	$y = a \times tDOC\% + b$	-3.17×10^{-3}	1.62	0.45	√
HIX	$y = \exp(a \times tDOC\% + b)$	6.21×10^{-3}	-4.43×10^{-1}	0.62	×
C2-Fmax/DOC	$y = a \times tDOC\% + b$	1.07×10^{-5}	1.29×10^{-4}	0.64	√

471 *Consistency corresponds to whether the extrapolated relationship at 100% tDOC falls within the reference river data
 472 from Sarawak: √—falls in the range, ×—falls out of the range.

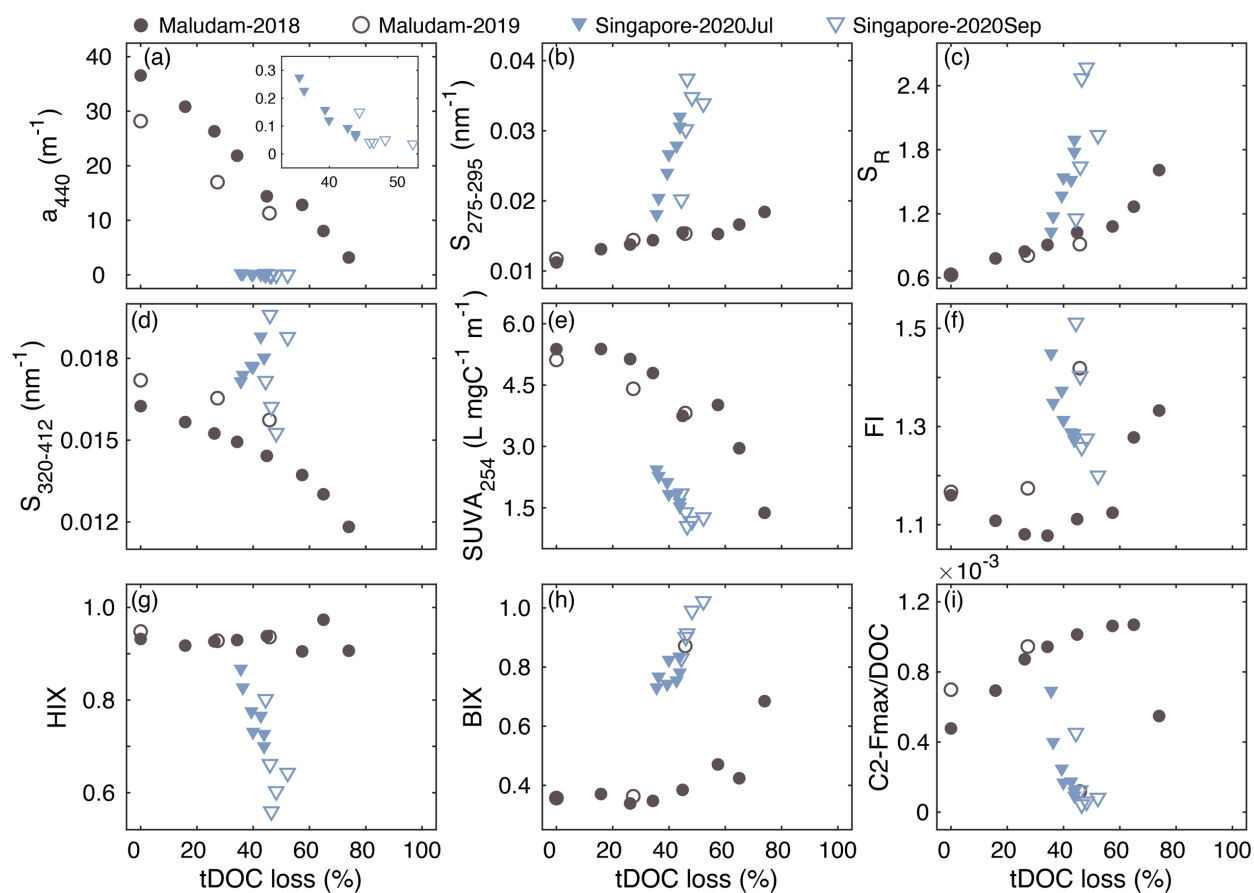
473

474 3.6 Relationships of optical properties to tDOC remineralization

475 Our isotope mass balance showed that the tDOC had experienced a varying extent of
 476 remineralization before reaching our sampling site. Unlike the strong relationships with tDOC%,
 477 none of the optical properties were related to the extent of tDOC remineralization, even though the
 478 extent of tDOC remineralization ranged from 7% to 75% during the SW Monsoon (Figure S4).
 479 This suggests that although most of the optical properties can be used as tracers of tDOC%, they
 480 do not appear to be sensitive to the extent of tDOC remineralization in the natural environment.
 481 We restricted this analysis to include only data from the SW Monsoon as this is the only season
 482 with sufficiently large tDOC input to quantify the remineralization percentage accurately. The
 483 absolute concentration of tDOC is much lower in other seasons, and small variations in $\delta^{13}C_{DIC}$
 484 can then result in a very large range of inferred percentage tDOC remineralization, which we
 485 consider to be inaccurate.

486 In contrast, most of the optical properties did show clear relationships to percentage tDOC loss in
 487 our laboratory photodegradation experiments, both with pure tDOC samples from a peatland-
 488 draining river (Maludam) and with coastal water samples from the Singapore Strait during the SW
 489 Monsoon (Figure 6). For Maludam river samples, CDOM a_{440} decreased linearly with tDOC loss
 490 while $S_{275-295}$ and S_R increased linearly by 64% and 156%, respectively (Figure 6a–c). $S_{320-412}$ and

501 SUVA₂₅₄ showed exponential decreases from ~ 0.016 to ~ 0.012 nm⁻¹ and from ~ 5.2 to ~ 1.5 L mg-
 502 C⁻¹ m⁻¹, respectively (Figure 6d–e). However, fluorescence properties showed more variability. FI
 503 first dropped by $\sim 10\%$ upon 30%–40% tDOC loss, after which it increased (Figure 6f). HIX
 504 always stayed at around 0.93 across the whole percent tDOC loss (Figure 6g) and BIX started to
 505 rise once tDOC loss exceeded 50% (Figure 6h). C2-Fmax/DOC exhibited a general increase of
 506 more than two times of the initial value. For the two coastal water samples from Singapore, we
 estimated tDOC loss by taking the prior natural tDOC remineralization (from our isotope mass
 balance) into account, and we conservatively assumed that all DOC lost during the incubation was
 tDOC, because marine DOC at our site is not very photo-sensitive (Zhou et al. 2021). Although
 only little DOC was remineralized in the coastal water samples, $S_{275-295}$ and S_R changed by more
 than twofold relative to the initial values, while SUVA₂₅₄, HIX and C2-Fmax/DOC decreased
 linearly to a smaller degree with percent tDOC loss. $S_{320-412}$ and BIX only changed slightly.



503
 504 Figure 6. Changes in optical properties as a function of the percentage loss of tDOC during pure photodegradation
 505 experiments for Singapore coastal water and water from a peatland-draining river in Sarawak (Maludam River).
 506 Unlike the patterns of optical properties against percent tDOC loss in natural coastal water, most of the parameters

507 did present certain correlations to tDOC loss in laboratory incubation purely under photo exposure, but the correlations
508 were different for different water types.

509

510 **4 Discussion**

511 4.1 Reliability of tDOC calculation

512 Carbon stable isotope measurements can provide strong insights into sources and biogeochemical
513 processing of DOM (Alling et al., 2008; Bauer & Bianchi, 2011; Lee et al., 2020). As DOM from
514 terrestrial source and marine environment possess distinctive carbon isotope compositions, the
515 $\delta^{13}\text{C}_{\text{DOC}}$ values are widely used as fingerprints to distinguish DOC from different sources based
516 on endmember mixing models (Humborg et al., 2017; Ye et al., 2018; Zhou et al., 2021). Our
517 estimated endmember $\delta^{13}\text{C}_{\text{DOC}}$ values (Table S2) conform to the generally reported ranges of -25%
518 to -32% and -21% to -22% for riverine and marine endmembers, respectively (Bauer, 2002;
519 Beaupré, 2015; Gandois et al., 2014). From our estimated endmember values for $\delta^{13}\text{C}_{\text{DOC}}$ and the
520 measured DOC concentrations in our coastal samples we could therefore use a mixing model to
521 estimate the remaining tDOC concentration (Section 2.5.2 and Text S1.1). Besides, it is known
522 that apart from physical mixing, biogeochemical processes including primary
523 production/remineralization, CaCO_3 dissolution/calcification and CO_2 outgassing/uptake, also
524 cause stoichiometrically constrained changes in DIC and TA, and can induce carbon isotope
525 fractionation (Zeebe & Wolf-Gladrow, 2001). In our case, the deviations in DIC and TA are
526 primarily caused by remineralization and CaCO_3 dissolution/calcification, while net CO_2
527 outgassing is expected within the Sunda Shelf (Kartadikaria et al., 2015; Wit et al., 2018; Zhou et
528 al., 2021).

529 Several previous studies have applied the stable carbon isotope mass balance approach to quantify
530 the contribution of terrestrial organic matter degradation to the observed DIC and $\delta^{13}\text{C}_{\text{DIC}}$ in
531 different regions (Humborg et al., 2017; Samanta et al., 2015; Su et al., 2020; Zhou et al., 2021)
532 For example, it was estimated from the depletion in $\delta^{13}\text{C}_{\text{DIC}}$ that annually 4.0 Tg terrestrial organic
533 matter is respired in the central and outer Laptev Sea in the Arctic (Humborg et al., 2017). Based
534 on a compiled dataset including DIC, $\delta^{13}\text{C}_{\text{DIC}}$, dissolved calcium and oxygen, it was found that
535 remineralization is the main cause of the deviation from conservative mixing in the Hooghly River

536 estuary in India (Samanta et al., 2015). Similarly, a mass balance calculation in the hypoxic zone
537 of the Pearl River estuary in China demonstrated that on average 35% of the total organic matter
538 remineralization was of terrestrial organic matter (Su et al., 2017), while the calculation in the
539 Chesapeake Bay in the US showed that autochthonous organic matter rather than terrestrially
540 derived organic matter dominated oxygen-consuming process (Su et al., 2020). The deviation of
541 measured $\delta^{13}\text{C}_{\text{DIC}}$ from its conservative mixing value in our dataset (around -1‰ during SW
542 Monsoon) is similar to the deviation observed in these previous studies, which suggests that our
543 mass balance calculation provides robust estimates of tDOC remineralization.

544 The riverine endmember values in the present analysis can be considered entirely contributed by
545 tDOC and terrigenous CDOM. On the one hand, DOM produced from phytoplankton or other
546 microbial processes always stayed at a steady and low level. This is demonstrated by stable $S_{320-412}$
547 values and low C5-Fmax largely around or even less than 0.05 RU for both coastal water and river
548 water (Figure 4d and data not shown), both of which did not show any seasonality (Figure 1f and
549 Figure 2e). The low $S_{320-412}$ and little signals of C5 are aligned with the annually low concentration
550 of chlorophyll-a which is possibly caused by limited light availability (Martin et al., 2021; Morgan
551 et al., 2020) and tidal mixing of the water column (Mayer & Pohlmann, 2014). Besides,
552 typically >95% of the terrigenous organic carbon in Southeast Asian peatland-draining rivers is in
553 form of DOC (Baum et al., 2007; Moore et al., 2011; Müller et al., 2015), and the small part of
554 transported POC can probably sink and accumulate in the sediment, thus the remineralization of
555 POC can hardly make a difference in the observed DIC and $\delta^{13}\text{C}_{\text{DIC}}$.

556 4.2 Preferential loss of CDOM compared to tDOC during natural remineralization

557 tDOC generally has a high content of chromophores, and CDOM in estuaries and coastal waters
558 is therefore often of terrestrial origin (Asmala et al., 2012; Chen et al., 2015; Osburn et al., 2016;
559 Santos et al., 2016). This characteristic provides the basis for using optical properties to study
560 tDOC. Absorption coefficients (a_λ) often show strong correlations with bulk DOC concentrations
561 in rivers, estuaries and coastal waters (Asmala et al., 2012; Fichot et al., 2016; Mann et al., 2016;
562 Martin et al., 2018; Stedmon et al., 2011). However, we also observed preferential removal of
563 CDOM compared to tDOC remineralization, although the difference was relatively modest (77%
564 versus 56% loss). This finding is consistent with previous work on biological and photochemical
565 processes of DOM for freshwater (Benner & Kaiser, 2011; Martin et al., 2018; Spencer, Stubbins,

566 et al., 2009) and coastal waters (Moran et al., 2000; Osburn et al., 2009). For example, the half-
567 life time of CDOM in the Mackenzie River was estimated to be shorter than that of DOC when the
568 river water was exposed to sunlight (Osburn et al., 2009). Similarly, removal of CDOM was found
569 to be 21% more than that of DOC in biodegradation incubations conducted with water from a
570 coastal estuary in Georgia after it was photo-exposed (Moran et al., 2000). Moreover, a large
571 decrease in a_{355}/DOC ratio against salinity was observed in waters from the Middle Atlantic Bight,
572 especially when the solar irradiance was higher (Del Vecchio & Blough, 2004b). A key mechanism
573 driving preferential CDOM loss is likely that aromatic structures in chromophores can be partly
574 oxidised to non-chromophoric DOC during biogeochemical processes, especially by reactive
575 oxygen species formed under photo exposure (Cory & Kling, 2018; Del Vecchio & Blough, 2002;
576 Vione et al., 2009). Furthermore, it is reported that photochemical reactions of specific molecules
577 of DOM, such as aromatic amino acids, could change DOM characteristics and possibly make the
578 products unavailable for microbes, thus inhibiting bacterial degradation processes (Amado et al.,
579 2015). Our finding that CDOM loss is greater than tDOC loss is therefore fully consistent with
580 previous experimental and observational research in other regions.

581 Pure biodegradation of Southeast Asian peatland DOM appears to be much too slow to account
582 for the observed remineralization (Nichols & Martin, 2021), while photodegradation can remove
583 large fractions of the tDOC and CDOM (Zhou et al., 2021). However, pure photochemical
584 remineralization is usually fairly slow in the natural environment due to the comparatively low
585 natural sunlight doses (Fichot & Benner, 2014; Osburn et al., 2009; Reader & Miller, 2012).
586 Therefore, it is most likely that interactive photo-stimulated biodegradation plays an important role
587 in tDOC remineralization and CDOM decomposition. Notably, although there is a large extent of
588 tDOC and CDOM removal, the tDOC and CDOM concentrations still showed a pattern of
589 conservative mixing at our study site. While this might appear to be contradictory, in fact this only
590 indicates that physical mixing over the salinity range observed at our site occurs faster than the
591 remineralization rate, and that the majority of the observed remineralization therefore takes place
592 upstream of our sampling site.

593 4.3 Accuracy of optical properties as tracers of tDOC content in natural water

594 DOM optical properties have been widely measured in estuarine and coastal environments, and it
595 is clear that they can be sensitive indicators of the presence of tDOC (Fichot & Benner, 2012;

596 Kaiser et al., 2017; Massicotte et al., 2017; Mizubayashi et al., 2013; Painter et al., 2018; Stedmon
597 & Nelson, 2015). Several environmental studies have also demonstrated that some optical
598 properties (a_λ and $S_{275-295}$) can be used to quantify tDOC concentration as calculated from lignin
599 phenols (Fichot & Benner, 2012; Fichot et al., 2016; Hernes & Benner, 2003; Lu et al., 2016;
600 Walker et al., 2013). However, lignin phenols are a small (typically 0.1–4% of DOC; Hernes et
601 al., 2007; Opsahl & Benner, 1997; Osburn et al., 2016) and potentially rather labile (Cao et al.,
602 2018; Hernes & Benner, 2003; Ronald Benner & Kaiser, 2011) fraction of tDOC, while terrigenous
603 CDOM and FDOM may also be preferentially removed relative to bulk tDOC (Benner & Kaiser,
604 2011; Moran et al., 2000; Osburn et al., 2009). Specifically, both lignin and CDOM/FDOM are
605 composed to a significant degree of aromatic moieties, which are especially photo-labile, while
606 most aliphatic compounds are less susceptible to photodegradation (Berggren et al., 2022; Opsahl
607 & Benner, 1998; Osburn et al., 2001; Schmitt-Kopplin et al., 1998). In contrast, aromatic
608 components are generally more recalcitrant to microbial processes (Kang & Mitchell, 2013). These
609 difference in reactivity can likely account for preferential removal of lignin phenols and of
610 CDOM/FDOM relative to the bulk tDOC. For example, it was reported that the removal of lignin
611 phenols and CDOM was more than twice as high as the loss of DOC during combined photo- and
612 biodegradation of water from Broad River in South Carolina in the US (Benner & Kaiser, 2011).
613 However, the degree to which optical properties are lost preferentially is likely dependent on the
614 relative rates of different degradation processes, which are poorly quantified in natural
615 environments. Therefore, it is still unclear how accurately these optical properties can trace total
616 tDOC when it is also being subjected to natural remineralization processes. In the present study,
617 we therefore used $\delta^{13}\text{C}_{\text{DOC}}$ to estimate tDOC concentration and $\delta^{13}\text{C}_{\text{DIC}}$ to estimate the extent of
618 prior tDOC remineralization. Our results provide robust statistical evidence that all the optical
619 properties typically used to identify tDOM are significantly related to tDOC% even when more
620 than half of tDOC has already been remineralized (Figure 5). However, the different properties
621 have variably strong relationships and differ in their sensitivity to tDOC in different parts of the
622 tDOC% range.

623 The strong linear relationship between a_{440} and tDOC% shows that CDOM absorption coefficients
624 can still be used to quantify tDOC in coastal water even when extensive remineralization has taken
625 place. However, the fact that we did observe preferential removal of CDOM relative to tDOC
626 (Figure 3e–f) underscores the fact that a_λ -tDOC relationships are sensitive to the extent of tDOM

627 biogeochemical degradation and must therefore change significantly across estuarine and coastal
628 gradients. In addition, the high variability of a_{440} in estuaries can result from the mixing of seawater
629 and different rivers with highly distinctive concentrations of tDOC and CDOM depending on the
630 catchment coverage of peatland (Rixen et al., 2022). Caution would therefore be needed in
631 attempting to calculate tDOC concentrations from a_{λ} when the range in remineralization might be
632 large and when the riverine influence is complex.

633 The non-linear relationships we observed for $S_{275-295}$ and S_R with tDOC% are consistent with
634 previous studies showing exponential relationships for $S_{275-295}$ with lignin phenol concentration
635 (Benner et al., 2005; Fichot & Benner, 2012) and linear correlation for S_R with carbon-normalized
636 lignin yield (Spencer et al., 2010). Besides, after extrapolating the fitting curve to salinity 0, the
637 relationships showed good consistency with tropical peatland river data, suggesting that unlike
638 CDOM absorption, these spectral slope-based properties maintain a constant relationship to
639 tDOC% even as tDOC is remineralized. Based on the r^2 and confidence intervals, both $S_{275-295}$ and
640 S_R show similar accuracy for quantifying tDOC% (Figure 5 and Table 2), resulting from the
641 relatively steady $S_{350-400}$ across the whole salinity gradient (data not shown), consistent with
642 previous research (Fichot & Benner, 2012). It is interesting to note that compared to $S_{275-295}$, the
643 slope ratio S_R shows less variability at mid-salinities in the data from Sarawak, suggesting that S_R
644 might be less sensitive to the mixing among different rivers (Figure 4d). However, in our time
645 series data from the Singapore Strait, $S_{275-295}$ and S_R were equally well related to tDOC% (Figure
646 5).

647 $SUVA_{254}$ is usually interpreted as a measure of DOM aromaticity, as shown by ^{13}C -NMR
648 measurements with organic matter from a variety of aquatic environments (Weishaar et al., 2003).
649 Moreover, $SUVA_{254}$ was recently proposed as a measure to distinguish between primarily
650 photochemically labile tDOC and bio-labile tDOC in the UniDOM biogeochemical modelling
651 framework (Anderson et al., 2019). Our study demonstrates that $SUVA_{254}$ is linearly related to
652 tDOC% and performs better than other CDOM measures as a quantitative tDOC tracer, given that
653 the relationship shows less scatter ($r^2 = 0.66$) and narrower confidence and prediction intervals
654 (Figure 5e). This is consistent with the robust positive relationships between $SUVA_{254}$ and the
655 fraction of humic substances obtained from a diverse range of watersheds in the US (Spencer et
656 al., 2012). We note that our $SUVA_{254}$ -tDOC% relationship extrapolates to the lower boundary of

657 available river data. While the true $SUVA_{254}$ for rivers on Sumatra is not known, this result likely
658 indicates some sensitivity of $SUVA_{254}$ to preferential CDOM loss during tDOC remineralization.
659 Our data cannot confirm whether reduction in $SUVA_{254}$ reflects the conversion of primarily photo-
660 labile tDOC to bio-labile structures as suggested in the UniDOM model (Anderson et al., 2019),
661 but they do suggest that $SUVA_{254}$ can provide a good measure of tDOC in coastal environments.

662 The fluorescence index (FI) and humification index (HIX) are also widely used as tDOC tracers
663 but mainly as qualitative indicators. It is suggested that when FI is less than 1.4, the DOC pool is
664 dominated by terrestrial matter, while FI larger than 1.4 indicates an increasing dominance of
665 microbially-derived DOC (Cory et al., 2010; McKnight et al., 2001). Our data show that FI has a
666 clear linear relationship with tDOC% (Figure 5f), which notably contrasts with the poor
667 relationship between FI and the proportion of humic substances in DOM reported from a river
668 basin in eastern Thailand (Kida et al., 2018). However, the formula of FI calculation is not strictly
669 fixed, depending on how fluorescence spectral correction is conducted (Cory & McKnight, 2005;
670 Cory et al., 2010; McKnight et al., 2001). Additionally, it has been suggested that FI changes by
671 at least 0.1 units when there is a source change in DOM (McKnight et al., 2001). It is clear that FI
672 can change up to 0.3 in the Singapore Strait over a range of tDOC% from 0 (during inter-monsoon
673 seasons) to ~60% (during the SW Monsoon). However, FI is also the most variable parameter in
674 the river data, with some rivers having FI values similar to the inter-monsoon data from the
675 Singapore Strait, despite carrying predominantly tDOC (Zhou et al., 2019). FI is therefore
676 potentially less useful as a tDOC tracer than the other optical properties.

677 It is expected that HIX rises along with tDOC% increase because it indicates humification level,
678 and humic substances are an important component of tDOC (Ohno, 2002; Zsolnay et al., 1999).
679 However, similar to FI, the HIX calculation is not identical in different studies (Birdwell & Engel,
680 2010; Inamdar et al., 2011; Lee et al., 2018; Ohno, 2002). We choose to use the formula after
681 inner-filtering correction (Ohno, 2002) as our dataset spans a large range of DOC concentrations.
682 HIX does show a clear relationship with tDOC%, but notably, the river data do not fall on the same
683 relationship extrapolated from the coastal water data. It is well known that humic substances can
684 be broken down after tDOC experiences biogeochemical processes, reducing the humification
685 level (Catalán et al., 2013; Hansen et al., 2016; Huguet et al., 2009; Wilske et al., 2020).
686 Nevertheless, some studies also report that DOM can be transformed to humified materials under
687 photo-exposure or during microbial degradation, thus causing HIX to increase (Chen & Jaffé,

688 2014; Garcia et al., 2018; Hansen et al., 2016; Kieber et al., 1997; Ortega-Retuerta et al., 2010).
689 The complex changing patterns during biogeochemical processes may make HIX insensitive above
690 a certain level of humification or tDOC%. For example, we note that HIX showed almost no
691 change during photo-exposure of the Maludam River samples (Figure 6g).

692 We additionally consider C2-Fmax/DOC, as it was used previously to estimate tDOC% for the
693 Sarawak data, assuming that there would be no preferential removal of C2 relative to bulk tDOC
694 over the small spatial scales of the estuaries in Sarawak (Zhou et al., 2019). Our new data from
695 Singapore correspond to a longer water residence time, providing more opportunity for preferential
696 removal of C2, which is expected to be fairly photo-labile (Grunert et al., 2021; Sankar et al.,
697 2019). Some other studies have investigated relationships between absolute Fmax values and
698 tDOC tracers such as lignin phenols (Osburn & Stedmon, 2011; Walker et al., 2013; Yang & Hur,
699 2014). However, given the substantial physical dilution, DOC normalization is appropriate. C2-
700 Fmax/DOC is thus analogous to SUVA₂₅₄. Our data confirm that this measure is able to quantify
701 tDOC% nearly as well as SUVA₂₅₄ across the large range seen in our Singapore Strait data, with
702 a strong correlation coefficient ($r^2=0.64$, Figure 5i). This agrees with the strong linear correlation
703 of C2 fluorescence to concentrations of lignin phenols obtained from Arctic rivers (Walker et al.,
704 2013).

705 In contrast to these optical measures associated with tDOC, neither S_{320–412} nor BIX were related
706 to tDOC%, and indeed showed little variation throughout our time series. The Singapore Strait
707 does not appear to experience large seasonality in phytoplankton production (Martin et al., 2022),
708 and the production and microbial processing of autochthonous DOC are likely closely coupled
709 year-round, with a relatively refractory marine DOC pool (Zhou et al., 2021). While our data thus
710 cannot evaluate how well these two optical properties can trace the presence of freshly produced
711 autochthonous DOC, our results do show that in the absence of fresh autochthonous DOC inputs,
712 they show fairly stable values even as the DOC pool receives highly variable amounts of additional
713 tDOC input (Figure 1f and Figure 2e).

714 Overall, our data thus demonstrate that all optical properties that are typically associated with
715 tDOC (a₄₄₀, S_{275–295}, S_R, SUVA₂₅₄, FI, HIX and C2-Fmax/DOC) are indeed quantitatively related
716 to tDOC% in coastal water, even after the tDOC has undergone a substantial degree of
717 remineralization. However, the optical properties differ in the shape of the relationship to tDOC%,

718 indicating differences in applicability. $S_{275-295}$, S_R and HIX show non-linear change with tDOC%,
719 which makes them very sensitive to small changes in tDOC concentration at low tDOC%, but
720 much less sensitive to tDOC% above a certain level (~40%–60%). On the other hand, a_{440} ,
721 $SUVA_{254}$, FI and C2-Fmax/DOC present linear behaviors. This means that they are less sensitive
722 than the non-linear-related indicators at low tDOC%, but they show a consistent ability to quantify
723 tDOC% at least within the range of 0–60%. Clearly, however, the preferential removal of CDOM
724 means that a_λ needs to be used cautiously for quantifying tDOC if the range in possible
725 remineralization extent is large. The fact that $SUVA_{254}$ and C2-Fmax/DOC are normalized to DOC
726 concentration appears to make these measures more robust, although the need for DOC
727 measurements makes these parameters less easy and less rapid to measure. Thus, it is essential to
728 understand basic characteristics of certain water samples and consider measurement limitations
729 before choosing appropriate optical indicators to quantify tDOC%.

730 4.4 Qualitative proxies of tDOC biogeochemical processes

731 Our carbon stable isotope mass balance shows clearly that a variable proportion of the original
732 tDOC was remineralized before reaching our site. It has previously been demonstrated that
733 biodegradation and UV irradiation can cause optical properties to change in different directions
734 and/or at different rates (Hansen et al., 2016; Helms et al., 2008; Lee et al., 2018). Subsequently,
735 such changes might allow one to use optical properties to diagnose certain biogeochemical
736 processes: for example, photochemical and microbial degradation of tDOC are reported to affect
737 S_R differently (Hansen et al., 2016; Helms et al., 2008), while photochemical degradation
738 consistently increases $S_{275-295}$ (Fichot & Benner, 2012; Helms et al., 2014; Zhou et al., 2021). Here,
739 we additionally tested whether the optical properties can also be used to infer the extent of natural
740 tDOC remineralization in the environment. However, unlike the strong relationships to tDOC%,
741 and despite spanning a range of 20–80% tDOC loss, none of the optical properties showed any
742 consistent trends with tDOC loss (Figure S4).

743 The fact that the optical properties show little change with tDOC loss could arise from the
744 complexity of biogeochemical processes in the environment, where photodegradation,
745 biodegradation, and their interactions take place simultaneously (Del Vecchio & Blough, 2002;
746 Fovet et al., 2020; Lønborg et al., 2010; Osburn et al., 2009; Ward et al., 2017). Generally,
747 photodegradation is considered to play a significant role in tDOC remineralization. Yet, the extent

748 and rate of photo-induced remineralization and optical property change can vary depending on
749 light intensities, irradiation wavelengths and specific origins of tDOC (Clark et al., 2020; Du et
750 al., 2016; Hansen et al., 2016; Lee et al., 2018; Moran et al., 2000). It has been shown that
751 biodegradation may cause optical properties of DOM to change less and possibly in an opposite
752 direction compared to photodegradation (Hansen et al., 2016; Hernes & Benner, 2003; Hur et al.,
753 2011; Lee et al., 2018). Microbial remineralization of tDOC is often significantly enhanced after
754 partial photodegradation (Hansen et al., 2016; Miller & Moran, 1997; Moran et al., 2000), but
755 conversely, photochemical reactions can also compete with microbial processes (Amado et al.,
756 2015; Ward et al., 2017). In natural coastal environments, photo-induced reactions and microbial
757 remineralization most likely always co-occur and interact at least to some degree. It is therefore
758 possible that different co-occurring remineralization processes result in more limited changes in
759 optical properties than those observed in single-process incubation experiments. A recent
760 experimental study showed that microbial and combined photochemical + microbial degradation
761 caused the optical properties of different plant leachates to converge over time despite large
762 differences in initial properties (Harfmann et al., 2019). Tropical peatland tDOM experiences
763 partial degradation within the peat dome before entering rivers (Gandois et al., 2014), so it is
764 possible that the optical properties of the riverine tDOM pool have already undergone “microbial
765 buffering” (Harfmann et al., 2019). Subsequent interactive photochemical and microbial
766 degradation might then only have a limited impact on CDOM and FDOM spectral characteristics,
767 consistent with our observations.

768 In the case of riverine tDOC from Southeast Asian peatlands, pure microbial remineralization
769 appears to be relatively slow and no clear alteration of optical properties was found in microbial
770 incubation experiments of 3–6 months duration (Nichols & Martin, 2021; Zhou et al., 2021). We
771 therefore compare our environmental data to results from pure photodegradation experiments. For
772 most parameters, especially $S_{275-295}$, S_R , and $SUVA_{254}$, we observed clear changes with consistent
773 direction (i.e., increasing or decreasing) as a function of tDOC loss for both the peatland-draining
774 river samples and the coastal water samples, and these changes are consistent with those reported
775 previously for tDOM photobleaching experiments (Du et al., 2016; Helms et al., 2013; Lee et al.,
776 2018; Magyan & Dempsey, 2021). Notably, we observed that the coastal water samples mostly
777 showed much more obvious changes in optical properties for a given %tDOC loss than the river
778 samples. The different rates of change are to be expected because coastal water samples contain

779 overall less CDOM and FDOM, and consist of a mixture of marine and terrestrial DOM, while the
780 river samples still consisted of tDOM even at the end of the incubations. The results of bio- and
781 photo-incubation for water from the peatland-draining river suggest that Southeast Asian peatland-
782 derived tDOM behaves similar to other highly humified photo-labile but bio-refractory tDOM
783 during remineralization (Chen & Jaffé, 2014; Dempsey et al., 2020). The fact that our
784 environmental data do not demonstrate such clear relationships between optical properties and
785 tDOC loss therefore suggests that natural tDOC remineralization in this region proceeds through
786 complex interactive degradation processes that do not leave clear signatures in the optical
787 properties. Further research would be valuable to understand how sequential and simultaneous
788 photo- and biodegradation of tDOM alter its optical properties, which can help to further our
789 interpretation of optical properties from natural water samples containing DOM from different
790 sources and after environmental processing.

791 **5 Conclusions**

792 In summary, our study shows that there is preferential removal of optically active tDOM relative
793 to total tDOC, but that DOM optical properties are nevertheless robust and potentially quantitative
794 indicators of tDOC% in coastal waters. The commonly used optical properties a_{440} , $S_{275-295}$, S_R ,
795 $SUVA_{254}$, FI, and HIX, as well as C2-Fmax/DOC, can all quantify tDOC% in coastal water, but
796 their relationships with tDOC% exhibit different shapes, accuracies and applicable ranges.
797 Specifically, CDOM spectral slope parameters are very sensitive to the presence of low levels of
798 tDOC, but show little further change once tDOC exceeds ~40% of total DOC. In contrast, $SUVA_{254}$
799 and C2-Fmax/DOC show linear relationships with tDOC contribution across a larger range of
800 values. However, none of the optical properties we considered showed a relationship to the extent
801 of tDOC remineralization, which we attribute to the likely complexity of multiple interacting
802 biogeochemical degradation processes.

803 **Acknowledgments**

804 We thank Oon Yee Woo, Su Ping Heng, Kristy Y.W. Chang, Ashleen S.Y. Tan, Molly A.
805 Moynihan, Robert S. Nichols, and Nikita Kaushal for help with field sampling and laboratory
806 analysis, and the captains and crew of *Dolphin Explorer* and R/V *Galaxea* for support in the field.
807 We are grateful to Richard Sanders for comments that helped to guide the analysis. This research
808 was funded by the Singapore Ministry of Education through Academic Research Fund Tier 2 grant

809 MOE-MOET2EP10121-0007 and by the National Research Foundation, Singapore, Prime
810 Minister's Office through grants MSRDP-P32 and NRF-NRI-2020-MESN.

811 Open Research

812 Processed data are available in the Supporting Information Data Set S1. The data that support the
813 findings of this study are openly available in Nanyang Technological University Data Repository
814 at <https://doi.org/10.21979/N9/Q1L9HR>.

815

816 References

- 817 Aksnes, D. L., Dupont, N., Staby, A., Fiksen, Ø., Kaartvedt, S., & Aure, J. (2009). Coastal water darkening and
818 implications for mesopelagic regime shifts in Norwegian fjords. *Marine Ecology Progress Series*, 387, 39-
819 49. [https://www.int-res.com/abstracts/meps/v387/p39-49/](https://www.int-res.com/abstracts/meps/v387/p39-49)
- 820 Alling, V., Humborg, C., Mörth, C.-M., Rahm, L., & Pollehne, F. (2008). Tracing terrestrial organic matter by $\delta^{34}\text{S}$
821 and $\delta^{13}\text{C}$ signatures in a subarctic estuary. 53(6), 2594-2602. <https://doi.org/10.4319/lo.2008.53.6.2594>
- 822 Alling, V., Porcelli, D., Mörth, C. M., Anderson, L. G., Sanchez-Garcia, L., Gustafsson, Ö., et al. (2012). Degradation
823 of terrestrial organic carbon, primary production and out-gassing of CO_2 in the Laptev and East Siberian
824 Seas as inferred from $\delta^{13}\text{C}$ values of DIC. *Geochimica et Cosmochimica Acta*, 95, 143-159.
825 <https://doi.org/https://doi.org/10.1016/j.gca.2012.07.028>
- 826 Amado, A. M., Cotner, J. B., Cory, R. M., Edhlund, B. L., & McNeill, K. (2015). Disentangling the Interactions
827 Between Photochemical and Bacterial Degradation of Dissolved Organic Matter: Amino Acids Play a Central
828 Role. *Microbial Ecology*, 69(3), 554-566. <https://doi.org/10.1007/s00248-014-0512-4>
- 829 Anderson, T. R., Rowe, E. C., Polimene, L., Tipping, E., Evans, C. D., Barry, C. D. G., et al. (2019). Unified concepts
830 for understanding and modelling turnover of dissolved organic matter from freshwaters to the ocean: the
831 UniDOM model. *Biogeochemistry*, 146(2), 105-123. <https://doi.org/10.1007/s10533-019-00621-1>
- 832 Antony, R., Willoughby, A. S., Grannas, A. M., Catanzano, V., Sleighter, R. L., Thamban, M., & Hatcher, P. G.
833 (2018). Photo-biochemical transformation of dissolved organic matter on the surface of the coastal East
834 Antarctic ice sheet. *Biogeochemistry*, 141(2), 229-247. <https://doi.org/10.1007/s10533-018-0516-0>
- 835 Asmala, E., Stedmon, C. A., & Thomas, D. N. (2012). Linking CDOM spectral absorption to dissolved organic carbon
836 concentrations and loadings in boreal estuaries. *Estuarine, Coastal and Shelf Science*, 111, 107-117.
837 <https://doi.org/https://doi.org/10.1016/j.ecss.2012.06.015>
- 838 Bauer, J. E. (2002). Chapter 8 - Carbon Isotopic Composition of DOM. In D. A. Hansell & C. A. Carlson (Eds.),
839 *Biogeochemistry of marine dissolved organic matter* (pp. 405-453). Academic Press.
840 <https://doi.org/https://doi.org/10.1016/B978-012323841-2/50010-5>
- 841 Bauer, J. E., & Bianchi, T. S. (2011). 5.02 - Dissolved Organic Carbon Cycling and Transformation. In E. Wolanski
842 & D. McLusky (Eds.), *Treatise on Estuarine and Coastal Science* (pp. 7-67). Academic Press.
843 <https://doi.org/https://doi.org/10.1016/B978-0-12-374711-2.00502-7>
- 844 Baum, A., Rixen, T., & Samiaji, J. (2007). Relevance of peat draining rivers in central Sumatra for the riverine input
845 of dissolved organic carbon into the ocean. *Estuarine, Coastal and Shelf Science*, 73(3), 563-570.
846 <https://doi.org/https://doi.org/10.1016/j.ecss.2007.02.012>
- 847 Beaupré, S. R. (2015). Chapter 6 - The Carbon Isotopic Composition of Marine DOC. In D. A. Hansell & C. A.
848 Carlson (Eds.), *Biogeochemistry of Marine Dissolved Organic Matter (Second Edition)* (pp. 335-368).
849 Academic Press. <https://doi.org/https://doi.org/10.1016/B978-0-12-405940-5.00006-6>
- 850 Bélanger, S., Xie, H., Krotkov, N., Larouche, P., Vincent, W. F., & Babin, M. (2006). Photomineralization of
851 terrigenous dissolved organic matter in Arctic coastal waters from 1979 to 2003: Interannual variability and
852 implications of climate change. *Global Biogeochemical Cycles*, 20(4).
853 <https://doi.org/https://doi.org/10.1029/2006GB002708>
- 854 Beleites, C., & Sergio, V. (2018). hyperSpec: a package to handle hyperspectral data sets in R. *R package version 0.99-
855 20180627*, URL <http://hyperspec.r-forge.r-project.org>.

- 856 Benner, R., & Kaiser, K. (2011). Biological and photochemical transformations of amino acids and lignin phenols in
857 riverine dissolved organic matter. *Biogeochemistry*, 102(1), 209-222. [https://doi.org/10.1007/s10533-010-](https://doi.org/10.1007/s10533-010-9435-4)
858 [9435-4](https://doi.org/10.1007/s10533-010-9435-4)
- 859 Benner, R., Louchouart, P., & Amon, R. M. W. (2005). Terrigenous dissolved organic matter in the Arctic Ocean and
860 its transport to surface and deep waters of the North Atlantic. *Global Biogeochemical Cycles*, 19(2).
861 <https://doi.org/https://doi.org/10.1029/2004GB002398>
- 862 Berggren, M., Guillemette, F., Bieroza, M., Buffam, I., Deininger, A., Hawkes, J. A., et al. (2022). Unified
863 understanding of intrinsic and extrinsic controls of dissolved organic carbon reactivity in aquatic ecosystems.
864 *Ecology*, 103(9), e3763. <https://doi.org/https://doi.org/10.1002/ecy.3763>
- 865 Birdwell, J. E., & Engel, A. S. (2010). Characterization of dissolved organic matter in cave and spring waters using
866 UV-Vis absorbance and fluorescence spectroscopy. *Organic Geochemistry*, 41(3), 270-280.
867 <https://doi.org/https://doi.org/10.1016/j.orggeochem.2009.11.002>
- 868 Cao, X., Aiken, G. R., Butler, K. D., Huntington, T. G., Balch, W. M., Mao, J., & Schmidt-Rohr, K. (2018). Evidence
869 for major input of riverine organic matter into the ocean. *Organic Geochemistry*, 116, 62-76.
870 <https://doi.org/https://doi.org/10.1016/j.orggeochem.2017.11.001>
- 871 Capelle, D. W., Kuzyk, Z. Z. A., Papakyriakou, T., Guéguen, C., Miller, L. A., & Macdonald, R. W. (2020). Effect of
872 terrestrial organic matter on ocean acidification and CO₂ flux in an Arctic shelf sea. *Progress in*
873 *Oceanography*, 185, 102319. <https://doi.org/https://doi.org/10.1016/j.pocean.2020.102319>
- 874 Cartisano, C. M., Del Vecchio, R., Bianca, M. R., & Blough, N. V. (2018). Investigating the sources and structure of
875 chromophoric dissolved organic matter (CDOM) in the North Pacific Ocean (NPO) utilizing optical
876 spectroscopy combined with solid phase extraction and borohydride reduction. *Marine Chemistry*, 204, 20-
877 35. <https://doi.org/https://doi.org/10.1016/j.marchem.2018.05.005>
- 878 Catalán, N., Obrador, B., Felip, M., & Pretus, J. L. (2013). Higher reactivity of allochthonous vs. autochthonous DOC
879 sources in a shallow lake. *Aquatic Sciences*, 75(4), 581-593. <https://doi.org/10.1007/s00027-013-0302-y>
- 880 Chen, M., & Jaffé, R. (2014). Photo- and bio-reactivity patterns of dissolved organic matter from biomass and soil
881 leachates and surface waters in a subtropical wetland. *Water Research*, 61, 181-190.
882 <https://doi.org/https://doi.org/10.1016/j.watres.2014.03.075>
- 883 Chen, Y., Liu, J., Zhang, X., & Blough, N. V. (2020). Time-Resolved Fluorescence Spectra of Untreated and Sodium
884 Borohydride-Reduced Chromophoric Dissolved Organic Matter. *Environmental Science & Technology*,
885 54(19), 12109-12118. <https://doi.org/10.1021/acs.est.0c03135>
- 886 Chen, Z., Doering, P. H., Ashton, M., & Orlando, B. A. (2015). Mixing behavior of colored dissolved organic matter
887 and its potential ecological implication in the Caloosahatchee River Estuary, Florida. *Estuaries and Coasts*,
888 38(5), 1706-1718. <https://doi.org/10.1007/s12237-014-9916-0>
- 889 Chin, Y.-P., Aiken, G., & O'Loughlin, E. (1994). Molecular weight, polydispersity, and spectroscopic properties of
890 aquatic humic substances. *Environmental Science & Technology*, 28(11), 1853-1858.
891 <https://doi.org/10.1021/es00060a015>
- 892 Ciais, P., Sabine, C., Bala, G., & Peters, W. (2013). Carbon and Other Biogeochemical Cycles. In T. F. Stocker, D.
893 Qin, G. K. Plattner, M. Tignor, S. K. Allen, J. Boschung, A. Nauels, Y. Xia, V. Bex, & P. M. Midgley (Eds.),
894 *Climate Change 2013: The Physical Science Basis. Contribution of Working Group I to the Fifth Assessment*
895 *Report of the Intergovernmental Panel on Climate Change* (pp. 465-570). Cambridge University Press.
896 <https://edepot.wur.nl/345905>
- 897 Clark, C. D., De Bruyn, W. J., Brahm, B., & Aiona, P. (2020). Optical properties of chromophoric dissolved organic
898 matter (CDOM) and dissolved organic carbon (DOC) levels in constructed water treatment wetland systems
899 in southern California, USA. *Chemosphere*, 247, 125906.
900 <https://doi.org/https://doi.org/10.1016/j.chemosphere.2020.125906>
- 901 Coble, P. G. (1996). Characterization of marine and terrestrial DOM in seawater using excitation-emission matrix
902 spectroscopy. *Marine Chemistry*, 51(4), 325-346. [https://doi.org/https://doi.org/10.1016/0304-](https://doi.org/https://doi.org/10.1016/0304-4203(95)00062-3)
903 [4203\(95\)00062-3](https://doi.org/https://doi.org/10.1016/0304-4203(95)00062-3)
- 904 Coble, P. G. (2007). Marine Optical Biogeochemistry: The Chemistry of Ocean Color. *Chemical Reviews*, 107(2),
905 402-418. <https://doi.org/10.1021/cr050350+>
- 906 Cory, R. M., & Kling, G. W. (2018). Interactions between sunlight and microorganisms influence dissolved organic
907 matter degradation along the aquatic continuum. *Limnology and Oceanography Letters*, 3(3), 102-116.
908 <https://doi.org/10.1002/lo2.10060>
- 909 Cory, R. M., & McKnight, D. M. (2005). Fluorescence spectroscopy reveals ubiquitous presence of oxidized and
910 reduced quinones in dissolved organic matter. *Environmental Science & Technology*, 39(21), 8142-8149.
911 <https://doi.org/10.1021/es0506962>

- 912 Cory, R. M., Miller, M. P., McKnight, D. M., Guerard, J. J., & Miller, P. L. (2010). Effect of instrument-specific
 913 response on the analysis of fulvic acid fluorescence spectra. *Limnology and Oceanography: Methods*, 8(2),
 914 67-78. <https://doi.org/https://doi.org/10.4319/lom.2010.8.67>
- 915 Dai, M., Yin, Z., Meng, F., Liu, Q., & Cai, W.-J. (2012). Spatial distribution of riverine DOC inputs to the ocean: an
 916 updated global synthesis. *Current Opinion in Environmental Sustainability*, 4(2), 170-178.
 917 <https://doi.org/https://doi.org/10.1016/j.cosust.2012.03.003>
- 918 Danhiez, F. P., Vantrepotte, V., Cauvin, A., Lebourg, E., & Loisel, H. (2017). Optical properties of chromophoric
 919 dissolved organic matter during a phytoplankton bloom. Implication for DOC estimates from CDOM
 920 absorption. *Limnology and Oceanography*, 62(4), 1409-1425.
 921 <https://doi.org/https://doi.org/10.1002/lno.10507>
- 922 Del Vecchio, R., & Blough, N. V. (2002). Photobleaching of chromophoric dissolved organic matter in natural waters:
 923 kinetics and modeling. *Marine Chemistry*, 78(4), 231-253. [https://doi.org/https://doi.org/10.1016/S0304-4203\(02\)00036-1](https://doi.org/https://doi.org/10.1016/S0304-4203(02)00036-1)
- 925 Del Vecchio, R., & Blough, N. V. (2004a). On the Origin of the Optical Properties of Humic Substances.
 926 *Environmental Science & Technology*, 38(14), 3885-3891. <https://doi.org/10.1021/es049912h>
- 927 Del Vecchio, R., & Blough, N. V. (2004b). Spatial and seasonal distribution of chromophoric dissolved organic matter
 928 and dissolved organic carbon in the Middle Atlantic Bight. *Marine Chemistry*, 89(1), 169-187.
 929 <https://doi.org/https://doi.org/10.1016/j.marchem.2004.02.027>
- 930 Dempsey, C. M., Brenttrup, J. A., Magyan, S., Knoll, L. B., Swain, H. M., Gaiser, E. E., et al. (2020). The relative
 931 importance of photodegradation and biodegradation of terrestrially derived dissolved organic carbon across
 932 four lakes of differing trophic status. *Biogeosciences*, 17(24), 6327-6340. <https://doi.org/10.5194/bg-17-6327-2020>
- 934 Dittmar, T. (2015). Chapter 7 - Reasons Behind the Long-Term Stability of Dissolved Organic Matter. In D. A. Hansell
 935 & C. A. Carlson (Eds.), *Biogeochemistry of Marine Dissolved Organic Matter (Second Edition)* (pp. 369-
 936 388). Academic Press. <https://doi.org/https://doi.org/10.1016/B978-0-12-405940-5.00007-8>
- 937 Du, Y., Zhang, Y., Chen, F., Chang, Y., & Liu, Z. (2016). Photochemical reactivities of dissolved organic matter
 938 (DOM) in a sub-alpine lake revealed by EEM-PARAFAC: An insight into the fate of allochthonous DOM in
 939 alpine lakes affected by climate change. *Science of The Total Environment*, 568, 216-225.
 940 <https://doi.org/https://doi.org/10.1016/j.scitotenv.2016.06.036>
- 941 Evans, C. D., Page, S. E., Jones, T., Moore, S., Gauci, V., Laiho, R., et al. (2014). Contrasting vulnerability of drained
 942 tropical and high-latitude peatlands to fluvial loss of stored carbon. *Global Biogeochemical Cycles*, 28(11),
 943 1215-1234. <https://doi.org/https://doi.org/10.1002/2013GB004782>
- 944 Fichot, C. G., & Benner, R. (2011). A novel method to estimate DOC concentrations from CDOM absorption
 945 coefficients in coastal waters. *Geophysical Research Letters*, 38(3), n/a-n/a.
 946 <https://doi.org/10.1029/2010gl046152>
- 947 Fichot, C. G., & Benner, R. (2012). The spectral slope coefficient of chromophoric dissolved organic matter (S₂₇₅₋₂₉₅)
 948 as a tracer of terrigenous dissolved organic carbon in river-influenced ocean margins. *Limnology and
 949 Oceanography*, 57(5), 1453-1466. <https://doi.org/10.4319/lo.2012.57.5.1453>
- 950 Fichot, C. G., & Benner, R. (2014). The fate of terrigenous dissolved organic carbon in a river-influenced ocean
 951 margin. *Global Biogeochemical Cycles*, 28(3), 300-318.
 952 <https://doi.org/https://doi.org/10.1002/2013GB004670>
- 953 Fichot, C. G., Benner, R., Kaiser, K., Shen, Y., Amon, R. M. W., Ogawa, H., & Lu, C.-J. (2016). Predicting Dissolved
 954 Lignin Phenol Concentrations in the Coastal Ocean from Chromophoric Dissolved Organic Matter (CDOM)
 955 Absorption Coefficients [Original Research]. *Frontiers in Marine Science*, 3(7).
 956 <https://doi.org/10.3389/fmars.2016.00007>
- 957 Fovet, O., Cooper, D. M., Jones, D. L., Jones, T. G., & Evans, C. D. (2020). Dynamics of dissolved organic matter in
 958 headwaters: comparison of headwater streams with contrasting DOM and nutrient composition. *Aquatic
 959 Sciences*, 82(2), 29. <https://doi.org/10.1007/s00027-020-0704-6>
- 960 Gandois, L., Teisserenc, R., Cobb, A. R., Chieng, H. I., Lim, L. B. L., Kamariah, A. S., et al. (2014). Origin,
 961 composition, and transformation of dissolved organic matter in tropical peatlands. *Geochimica et
 962 Cosmochimica Acta*, 137, 35-47. <https://doi.org/https://doi.org/10.1016/j.gca.2014.03.012>
- 963 Garcia, R. D., Diéguez, M. d. C., Gereá, M., Garcia, P. E., & Reissig, M. (2018). Characterisation and reactivity
 964 continuum of dissolved organic matter in forested headwater catchments of Andean Patagonia. *Freshwater
 965 Biology*, 63(9), 1049-1062. <https://doi.org/https://doi.org/10.1111/fwb.13114>
- 966 Gran, G. (1952). Determination of the equivalence point in potentiometric titrations. Part II. *The Analyst*, 77(920),
 967 661. <https://doi.org/10.1039/an9527700661>

- 968 Green, S. A., & Blough, N. V. (1994). Optical absorption and fluorescence properties of chromophoric dissolved
 969 organic matter in natural waters. *Limnology and Oceanography*, 39(8), 1903-1916.
 970 <https://doi.org/https://doi.org/10.4319/lo.1994.39.8.1903>
- 971 Grunert, B. K., Tzortziou, M., Neale, P., Menendez, A., & Hernes, P. (2021). DOM degradation by light and microbes
 972 along the Yukon River-coastal ocean continuum. *Scientific Reports*, 11(1), 10236.
 973 <https://doi.org/10.1038/s41598-021-89327-9>
- 974 Hansen, A. M., Kraus, T. E. C., Pellerin, B. A., Fleck, J. A., Downing, B. D., & Bergamaschi, B. A. (2016). Optical
 975 properties of dissolved organic matter (DOM): Effects of biological and photolytic degradation. *Limnology
 976 and Oceanography*, 61(3), 1015-1032. <https://doi.org/10.1002/lno.10270>
- 977 Harfmann, J. L., Guillemette, F., Kaiser, K., Spencer, R. G. M., Chuang, C.-Y., & Hernes, P. J. (2019). Convergence
 978 of Terrestrial Dissolved Organic Matter Composition and the Role of Microbial Buffering in Aquatic
 979 Ecosystems. *Journal of Geophysical Research: Biogeosciences*, 124(10), 3125-3142.
 980 <https://doi.org/https://doi.org/10.1029/2018JG004997>
- 981 Harun, S., Baker, A., Bradley, C., & Pinay, G. (2016). Spatial and seasonal variations in the composition of dissolved
 982 organic matter in a tropical catchment: the Lower Kinabatangan River, Sabah, Malaysia
 983 [10.1039/C5EM00462D]. *Environmental Science: Processes & Impacts*, 18(1), 137-150.
 984 <https://doi.org/10.1039/C5EM00462D>
- 985 Hedges, J. I., Keil, R. G., & Benner, R. (1997). What happens to terrestrial organic matter in the ocean? *Organic
 986 Geochemistry*, 27(5), 195-212. [https://doi.org/https://doi.org/10.1016/S0146-6380\(97\)00066-1](https://doi.org/https://doi.org/10.1016/S0146-6380(97)00066-1)
- 987 Helms, J. R., Mao, J., Stubbins, A., Schmidt-Rohr, K., Spencer, R. G. M., Hernes, P. J., & Mopper, K. (2014). Loss
 988 of optical and molecular indicators of terrigenous dissolved organic matter during long-term photobleaching.
 989 *Aquatic Sciences*, 76(3), 353-373. <https://doi.org/10.1007/s00027-014-0340-0>
- 990 Helms, J. R., Stubbins, A., Perdue, E. M., Green, N. W., Chen, H., & Mopper, K. (2013). Photochemical bleaching of
 991 oceanic dissolved organic matter and its effect on absorption spectral slope and fluorescence. *Marine
 992 Chemistry*, 155, 81-91. <https://doi.org/https://doi.org/10.1016/j.marchem.2013.05.015>
- 993 Helms, J. R., Stubbins, A., Ritchie, J. D., Minor, E. C., Kieber, D. J., & Mopper, K. (2008). Absorption spectral slopes
 994 and slope ratios as indicators of molecular weight, source, and photobleaching of chromophoric dissolved
 995 organic matter. *Limnology and Oceanography*, 53(3), 955-969. <https://doi.org/10.4319/lo.2008.53.3.0955>
- 996 Hernes, P. J., & Benner, R. (2003). Photochemical and microbial degradation of dissolved lignin phenols: Implications
 997 for the fate of terrigenous dissolved organic matter in marine environments. *Journal of Geophysical
 998 Research: Oceans*, 108(C9). <https://doi.org/10.1029/2002jc001421>
- 999 Huang, T. H., Chen, C. T. A., Tseng, H. C., Lou, J. Y., Wang, S. L., Yang, L., et al. (2017). Riverine carbon fluxes to
 1000 the South China Sea. *Journal of Geophysical Research: Biogeosciences*, 122(5), 1239-1259.
 1001 <https://doi.org/https://doi.org/10.1002/2016JG003701>
- 1002 Huguet, A., Vacher, L., Relexans, S., Saubusse, S., Froidefond, J. M., & Parlanti, E. (2009). Properties of fluorescent
 1003 dissolved organic matter in the Gironde Estuary. *Organic Geochemistry*, 40(6), 706-719.
 1004 <https://doi.org/https://doi.org/10.1016/j.orggeochem.2009.03.002>
- 1005 Humborg, C., Geibel, M. C., Anderson, L. G., Björk, G., Mörth, C.-M., Sundbom, M., et al. (2017). Sea-air exchange
 1006 patterns along the central and outer East Siberian Arctic Shelf as inferred from continuous CO₂, stable
 1007 isotope, and bulk chemistry measurements. *Global Biogeochemical Cycles*, 31(7), 1173-1191.
 1008 <https://doi.org/https://doi.org/10.1002/2017GB005656>
- 1009 Hur, J., Jung, K.-Y., & Schlautman, M. A. (2011). Altering the characteristics of a leaf litter-derived humic substance
 1010 by adsorptive fractionation versus simulated solar irradiation. *Water Research*, 45(18), 6217-6226.
 1011 <https://doi.org/https://doi.org/10.1016/j.watres.2011.09.023>
- 1012 Hur, J., Williams, M. A., & Schlautman, M. A. (2006). Evaluating spectroscopic and chromatographic techniques to
 1013 resolve dissolved organic matter via end member mixing analysis. *Chemosphere*, 63(3), 387-402.
 1014 <https://doi.org/https://doi.org/10.1016/j.chemosphere.2005.08.069>
- 1015 Inamdar, S., Singh, S., Dutta, S., Levia, D., Mitchell, M., Scott, D., et al. (2011). Fluorescence characteristics and
 1016 sources of dissolved organic matter for stream water during storm events in a forested mid-Atlantic
 1017 watershed. *Journal of Geophysical Research: Biogeosciences*, 116(G3).
 1018 <https://doi.org/https://doi.org/10.1029/2011JG001735>
- 1019 Jaffé, R., Cawley, K. M., & Yamashita, Y. (2014). Applications of Excitation Emission Matrix Fluorescence with
 1020 Parallel Factor Analysis (EEM-PARAFAC) in Assessing Environmental Dynamics of Natural Dissolved
 1021 Organic Matter (DOM) in Aquatic Environments: A Review. In *Advances in the Physicochemical
 1022 Characterization of Dissolved Organic Matter: Impact on Natural and Engineered Systems* (Vol. 1160, pp.
 1023 27-73). American Chemical Society. <https://doi.org/doi:10.1021/bk-2014-1160.ch003>

- 1024 10.1021/bk-2014-1160.ch003
- 1025 Kaiser, K., Benner, R., & Amon, R. M. W. (2017). The fate of terrigenous dissolved organic carbon on the Eurasian
1026 shelves and export to the North Atlantic. *Journal of Geophysical Research: Oceans*, 122(1), 4-22.
1027 <https://doi.org/https://doi.org/10.1002/2016JC012380>
- 1028 Kang, P.-G., & Mitchell, M. J. (2013). Bioavailability and size-fraction of dissolved organic carbon, nitrogen, and
1029 sulfur at the Arbutus Lake watershed, Adirondack Mountains, NY. *Biogeochemistry*, 115(1), 213-234.
1030 <https://doi.org/10.1007/s10533-013-9829-1>
- 1031 Karen, L. B.-N., & Mary Ann, M. (1999). Photochemical formation of biologically available nitrogen from dissolved
1032 humic substances in coastal marine systems. *Aquatic Microbial Ecology*, 18(3), 285-292. [https://www.int-](https://www.int-res.com/abstracts/ame/v18/n3/p285-292/)
1033 [res.com/abstracts/ame/v18/n3/p285-292/](https://www.int-res.com/abstracts/ame/v18/n3/p285-292/)
- 1034 Kartadikaria, A. R., Watanabe, A., Nadaoka, K., Adi, N. S., Prayitno, H. B., Soemorumekso, S., et al. (2015). CO₂
1035 sink/source characteristics in the tropical Indonesian seas. *Journal of Geophysical Research: Oceans*,
1036 120(12), 7842-7856. <https://doi.org/https://doi.org/10.1002/2015JC010925>
- 1037 Kida, M., Fujitake, N., Suchewaboripont, V., Pongparn, S., Tomotsune, M., Kondo, M., et al. (2018). Contribution
1038 of humic substances to dissolved organic matter optical properties and iron mobilization. *Aquatic Sciences*,
1039 80(3), 26. <https://doi.org/10.1007/s00027-018-0578-z>
- 1040 Kieber, R. J., Hydro, L. H., & Seaton, P. J. (1997). Photooxidation of triglycerides and fatty acids in seawater:
1041 Implication toward the formation of marine humic substances. *Limnology and Oceanography*, 42(6), 1454-
1042 1462. <https://doi.org/https://doi.org/10.4319/lo.1997.42.6.1454>
- 1043 Kowalczyk, P., Tilstone, G. H., Zabłocka, M., Röttgers, R., & Thomas, R. (2013). Composition of dissolved organic
1044 matter along an Atlantic Meridional Transect from fluorescence spectroscopy and Parallel Factor Analysis.
1045 *Marine Chemistry*, 157, 170-184. <https://doi.org/https://doi.org/10.1016/j.marchem.2013.10.004>
- 1046 Lawaetz, A. J., & Stedmon, C. A. (2009). Fluorescence Intensity Calibration Using the Raman Scatter Peak of Water.
1047 *Applied Spectroscopy*, 63(8), 936-940. <https://doi.org/10.1366/000370209788964548>
- 1048 Lee, M.-H., Osburn, C. L., Shin, K.-H., & Hur, J. (2018). New insight into the applicability of spectroscopic indices
1049 for dissolved organic matter (DOM) source discrimination in aquatic systems affected by biogeochemical
1050 processes. *Water Research*, 147, 164-176. <https://doi.org/https://doi.org/10.1016/j.watres.2018.09.048>
- 1051 Lee, S. A., Kim, T. H., & Kim, G. (2020). Tracing terrestrial versus marine sources of dissolved organic carbon in a
1052 coastal bay using stable carbon isotopes. *Biogeosciences*, 17(1), 135-144. [https://doi.org/10.5194/bg-17-135-](https://doi.org/10.5194/bg-17-135-2020)
1053 [2020](https://doi.org/10.5194/bg-17-135-2020)
- 1054 Letscher, R. T., Hansell, D. A., & Kadko, D. (2011). Rapid removal of terrigenous dissolved organic carbon over the
1055 Eurasian shelves of the Arctic Ocean. *Marine Chemistry*, 123(1), 78-87.
1056 <https://doi.org/https://doi.org/10.1016/j.marchem.2010.10.002>
- 1057 Lønborg, C., Alvarez-Salgado, X. A., Davidson, K., Martínez-García, S., & Teira, E. (2010). Assessing the microbial
1058 bioavailability and degradation rate constants of dissolved organic matter by fluorescence spectroscopy in
1059 the coastal upwelling system of the Ría de Vigo. *Marine Chemistry*, 119(1), 121-129.
1060 <https://doi.org/https://doi.org/10.1016/j.marchem.2010.02.001>
- 1061 Louchouart, P., Opsahl, S., & Benner, R. (2000). Isolation and Quantification of Dissolved Lignin from Natural
1062 Waters Using Solid-Phase Extraction and GC/MS. *Analytical Chemistry*, 72(13), 2780-2787.
1063 <https://doi.org/10.1021/ac9912552>
- 1064 Lu, C.-J., Benner, R., Fichot, C. G., Fukuda, H., Yamashita, Y., & Ogawa, H. (2016). Sources and Transformations
1065 of Dissolved Lignin Phenols and Chromophoric Dissolved Organic Matter in Otsuchi Bay, Japan [Original
1066 Research]. *Frontiers in Marine Science*, 3(85). <https://doi.org/10.3389/fmars.2016.00085>
- 1067 Magyan, S., & Dempsey, C. M. (2021). The role of time and mixing in the degradation of terrestrial derived dissolved
1068 organic carbon in lakes of varying trophic status. *Journal of Photochemistry and Photobiology*, 8, 100065.
1069 <https://doi.org/https://doi.org/10.1016/j.jpap.2021.100065>
- 1070 Mann, P. J., Spencer, R. G. M., Hernes, P. J., Six, J., Aiken, G. R., Tank, S. E., et al. (2016). Pan-Arctic Trends in
1071 Terrestrial Dissolved Organic Matter from Optical Measurements [Original Research]. 4(25).
1072 <https://doi.org/10.3389/feart.2016.00025>
- 1073 Martin, P., Cherukuru, N., Tan, A. S. Y., Sanwlani, N., Mujahid, A., & Müller, M. (2018). Distribution and cycling
1074 of terrigenous dissolved organic carbon in peatland-draining rivers and coastal waters of Sarawak, Borneo.
1075 *Biogeosciences*, 15(22), 6847-6865. <https://doi.org/10.5194/bg-15-6847-2018>
- 1076 Martin, P., Moynihan, M. A., Chen, S., Woo, O. Y., Zhou, Y., Nichols, R. S., et al. (2022). Monsoon-driven
1077 biogeochemical dynamics in an equatorial shelf sea: Time-series observations in the Singapore Strait.
1078 *Estuarine, Coastal and Shelf Science*, 270, 107855.
1079 <https://doi.org/https://doi.org/10.1016/j.ecss.2022.107855>

- 1080 Martin, P., Sanwlani, N., Lee, T. W. Q., Wong, J. M. C., Chang, K. Y. W., Wong, E. W. S., & Liew, S. C. (2021).
 1081 Dissolved organic matter from tropical peatlands reduces shelf sea light availability in the Singapore Strait,
 1082 Southeast Asia. *Marine Ecology Progress Series*, 672, 89-109. [https://www.int-](https://www.int-res.com/abstracts/meps/v672/p89-109/)
 1083 [res.com/abstracts/meps/v672/p89-109/](https://www.int-res.com/abstracts/meps/v672/p89-109/)
- 1084 Massicotte, P., Asmala, E., Stedmon, C., & Markager, S. (2017). Global distribution of dissolved organic matter along
 1085 the aquatic continuum: Across rivers, lakes and oceans. *Science of The Total Environment*, 609, 180-191.
 1086 <https://doi.org/https://doi.org/10.1016/j.scitotenv.2017.07.076>
- 1087 Mayer, B., & Pohlmann, T. (2014). Simulation of organic pollutants: First step towards an adaptation to the Malacca
 1088 Strait. *Asian Journal of Water, Environment and Pollution*, 11, 75-86.
- 1089 Mayer, B., Siegel, H., Gerth, M., Pohlmann, T., Stottmeister, I., Putri, M., & Setiawan, A. (2022). 2 - Physical
 1090 environment of the Indonesian Seas with focus on the western region. In T. C. Jennerjahn, T. Rixen, H. E.
 1091 Irianto, & J. Samiaji (Eds.), *Science for the Protection of Indonesian Coastal Ecosystems (SPICE)* (pp. 13-
 1092 43). Elsevier. <https://doi.org/https://doi.org/10.1016/B978-0-12-815050-4.00007-9>
- 1093 McKnight, D. M., Boyer, E. W., Westerhoff, P. K., Doran, P. T., Kulbe, T., & Andersen, D. T. (2001).
 1094 Spectrofluorometric characterization of dissolved organic matter for indication of precursor organic material
 1095 and aromaticity. *Limnology and Oceanography*, 46(1), 38-48. <https://doi.org/10.4319/lo.2001.46.1.0038>
- 1096 Medeiros, P. M., Seidel, M., Niggemann, J., Spencer, R. G. M., Hernes, P. J., Yager, P. L., et al. (2016). A novel
 1097 molecular approach for tracing terrigenous dissolved organic matter into the deep ocean. *Global*
 1098 *Biogeochemical Cycles*, 30(5), 689-699. <https://doi.org/https://doi.org/10.1002/2015GB005320>
- 1099 Meyers-Schulte, K. J., & Hedges, J. I. (1986). Molecular evidence for a terrestrial component of organic matter
 1100 dissolved in ocean water. *Nature*, 321(6065), 61-63. <https://doi.org/10.1038/321061a0>
- 1101 Miller, W. L., & Moran, M. A. (1997). Interaction of photochemical and microbial processes in the degradation of
 1102 refractory dissolved organic matter from a coastal marine environment. *Limnology and Oceanography*, 42(6),
 1103 1317-1324. <https://doi.org/https://doi.org/10.4319/lo.1997.42.6.1317>
- 1104 Mizubayashi, K., Kuwahara, V. S., Segaran, T. C., Zaleha, K., Effendy, A. W. M., Kushairi, M. R. M., & Toda, T.
 1105 (2013). Monsoon variability of ultraviolet radiation (UVR) attenuation and bio-optical factors in the Asian
 1106 tropical coral-reef waters. *Estuarine, Coastal and Shelf Science*, 126, 34-43.
 1107 <https://doi.org/https://doi.org/10.1016/j.ecss.2013.04.002>
- 1108 Moore, S., Gauci, V., Evans, C. D., & Page, S. E. (2011). Fluvial organic carbon losses from a Bornean blackwater
 1109 river. *Biogeosciences*, 8(4), 901-909. <https://doi.org/10.5194/bg-8-901-2011>
- 1110 Moran, M. A., Sheldon Jr., W. M., & Zepp, R. G. (2000). Carbon loss and optical property changes during long-term
 1111 photochemical and biological degradation of estuarine dissolved organic matter. *Limnology and*
 1112 *Oceanography*, 45(6), 1254-1264. <https://doi.org/https://doi.org/10.4319/lo.2000.45.6.1254>
- 1113 Morgan, K. M., Moynihan, M. A., Sanwlani, N., & Switzer, A. D. (2020). Light Limitation and Depth-Variable
 1114 Sedimentation Drives Vertical Reef Compression on Turbid Coral Reefs [Original Research]. *Frontiers in*
 1115 *Marine Science*, 7. <https://doi.org/10.3389/fmars.2020.571256>
- 1116 Müller, D., Warneke, T., Rixen, T., Müller, M., Jamahari, S., Denis, N., et al. (2015). Lateral carbon fluxes and
 1117 CO₂ outgassing from a tropical peat-draining river. *Biogeosciences*, 12(20), 5967-5979.
 1118 <https://doi.org/10.5194/bg-12-5967-2015>
- 1119 Murphy, K. R., Stedmon, C. A., Graeber, D., & Bro, R. (2013). Fluorescence spectroscopy and multi-way techniques.
 1120 PARAFAC [10.1039/C3AY41160E]. *Analytical Methods*, 5(23), 6557-6566.
 1121 <https://doi.org/10.1039/C3AY41160E>
- 1122 Murphy, K. R., Stedmon, C. A., Waite, T. D., & Ruiz, G. M. (2008). Distinguishing between terrestrial and
 1123 autochthonous organic matter sources in marine environments using fluorescence spectroscopy. *Marine*
 1124 *Chemistry*, 108(1), 40-58. <https://doi.org/https://doi.org/10.1016/j.marchem.2007.10.003>
- 1125 Nichols, R. S., & Martin, P. (2021). Low Biodegradability of Dissolved Organic Matter From Southeast Asian Peat-
 1126 Draining Rivers. *Journal of Geophysical Research: Biogeosciences*, 126(6), e2020JG006182.
 1127 <https://doi.org/https://doi.org/10.1029/2020JG006182>
- 1128 Ohno, T. (2002). Fluorescence Inner-Filtering Correction for Determining the Humification Index of Dissolved
 1129 Organic Matter. *Environmental Science & Technology*, 36(4), 742-746. <https://doi.org/10.1021/es0155276>
- 1130 Opsahl, S., & Benner, R. (1997). Distribution and cycling of terrigenous dissolved organic matter in the ocean. *Nature*,
 1131 386(6624), 480-482. <https://doi.org/10.1038/386480a0>
- 1132 Opsahl, S., & Benner, R. (1998). Photochemical reactivity of dissolved lignin in river and ocean waters. *Limnology*
 1133 *and Oceanography*, 43(6), 1297-1304. <https://doi.org/https://doi.org/10.4319/lo.1998.43.6.1297>

- 1134 Opsahl, S. P., & Zepp, R. G. (2001). Photochemically-induced alteration of stable carbon isotope ratios ($\delta^{13}\text{C}$) in
1135 terrigenous dissolved organic carbon. *Geophysical Research Letters*, 28(12), 2417-2420.
1136 <https://doi.org/10.1029/2000gl012686>
- 1137 Ortega-Retuerta, E., Reche, I., Pulido-Villena, E., Agustí, S., & Duarte, C. M. (2010). Distribution and photoreactivity
1138 of chromophoric dissolved organic matter in the Antarctic Peninsula (Southern Ocean). *Marine Chemistry*,
1139 118(3), 129-139. <https://doi.org/10.1016/j.marchem.2009.11.008>
- 1140 Osburn, C. L., Boyd, T. J., Montgomery, M. T., Bianchi, T. S., Coffin, R. B., & Paerl, H. W. (2016). Optical proxies
1141 for terrestrial dissolved organic matter in estuaries and coastal Waters [Original Research]. *Frontiers in*
1142 *Marine Science*, 2(127). <https://doi.org/10.3389/fmars.2015.00127>
- 1143 Osburn, C. L., Morris, D. P., Thorn, K. A., & Moeller, R. E. (2001). Chemical and optical changes in freshwater
1144 dissolved organic matter exposed to solar radiation. *Biogeochemistry*, 54(3), 251-278.
1145 <https://doi.org/10.1023/A:1010657428418>
- 1146 Osburn, C. L., Retamal, L., & Vincent, W. F. (2009). Photoreactivity of chromophoric dissolved organic matter
1147 transported by the Mackenzie River to the Beaufort Sea. *Marine Chemistry*, 115(1), 10-20.
1148 <https://doi.org/10.1016/j.marchem.2009.05.003>
- 1149 Osburn, C. L., & Stedmon, C. A. (2011). Linking the chemical and optical properties of dissolved organic matter in
1150 the Baltic-North Sea transition zone to differentiate three allochthonous inputs. *Marine Chemistry*, 126(1),
1151 281-294. <https://doi.org/10.1016/j.marchem.2011.06.007>
- 1152 Painter, S. C., Lapworth, D. J., Woodward, E. M. S., Kroeger, S., Evans, C. D., Mayor, D. J., & Sanders, R. J. (2018).
1153 Terrestrial dissolved organic matter distribution in the North Sea. *Science of The Total Environment*, 630,
1154 630-647. <https://doi.org/10.1016/j.scitotenv.2018.02.237>
- 1155 Qualls, R. G., & Richardson, C. J. (2003). Factors controlling concentration, export, and decomposition of dissolved
1156 organic nutrients in the Everglades of Florida. *Biogeochemistry*, 62(2), 197-229.
1157 <https://doi.org/10.1023/A:1021150503664>
- 1158 Raymond, P. A., & Spencer, R. G. M. (2015). Chapter 11 - Riverine DOM. In D. A. Hansell & C. A. Carlson (Eds.),
1159 *Biogeochemistry of Marine Dissolved Organic Matter (Second Edition)* (pp. 509-533). Academic Press.
1160 <https://doi.org/10.1016/B978-0-12-405940-5.00011-X>
- 1161 Reader, H. E., & Miller, W. L. (2012). Variability of carbon monoxide and carbon dioxide apparent quantum yield
1162 spectra in three coastal estuaries of the South Atlantic Bight. *Biogeosciences*, 9(11), 4279-4294.
1163 <https://doi.org/10.5194/bg-9-4279-2012>
- 1164 Rixen, T., Wit, F., Hutahaean, A. A., Schlüter, A., Baum, A., Klemme, A., et al. (2022). 4 - Carbon cycle in tropical
1165 peatlands and coastal seas. In T. C. Jennerjahn, T. Rixen, H. E. Irianto, & J. Samiaji (Eds.), *Science for the*
1166 *Protection of Indonesian Coastal Ecosystems (SPICE)* (pp. 83-142). Elsevier.
1167 <https://doi.org/10.1016/B978-0-12-815050-4.00011-0>
- 1168 Ronald Benner, & Kaiser, K. (2011). Biological and photochemical transformations of amino acids and lignin phenols
1169 in riverine dissolved organic matter. *Biogeochemistry*, 102(1-3), 209-222.
1170 <https://doi.org/10.1007/s10533-010-9435-4>
- 1171 Samanta, S., Dalai, T. K., Pattanaik, J. K., Rai, S. K., & Mazumdar, A. (2015). Dissolved inorganic carbon (DIC) and
1172 its $\delta^{13}\text{C}$ in the Ganga (Hooghly) River estuary, India: Evidence of DIC generation via organic carbon
1173 degradation and carbonate dissolution. *Geochimica et Cosmochimica Acta*, 165, 226-248.
1174 <https://doi.org/10.1016/j.gca.2015.05.040>
- 1175 Sankar, M. S., Dash, P., Singh, S., Lu, Y., Mercer, A. E., & Chen, S. (2019). Effect of photo-biodegradation and
1176 biodegradation on the biogeochemical cycling of dissolved organic matter across diverse surface water
1177 bodies. *Journal of Environmental Sciences*, 77, 130-147.
1178 <https://doi.org/10.1016/j.jes.2018.06.021>
- 1179 Santos, L., Pinto, A., Filipe, O., Cunha, Â., Santos, E. B. H., & Almeida, A. (2016). Insights on the Optical Properties
1180 of Estuarine DOM - Hydrological and Biological Influences. *PloS one*, 11(5), e0154519-e0154519.
1181 <https://doi.org/10.1371/journal.pone.0154519>
- 1182 Schmitt-Kopplin, P., Hertkorn, N., Schulten, H.-R., & Kettrup, A. (1998). Structural Changes in a Dissolved Soil
1183 Humic Acid during Photochemical Degradation Processes under O₂ and N₂ Atmosphere. *Environmental*
1184 *Science & Technology*, 32(17), 2531-2541. <https://doi.org/10.1021/es970636z>
- 1185 Semiletov, I., Pipko, I., Gustafsson, Ö., Anderson, L. G., Sergienko, V., Pugach, S., et al. (2016). Acidification of East
1186 Siberian Arctic Shelf waters through addition of freshwater and terrestrial carbon. *Nature Geoscience*, 9(5),
1187 361-365. <https://doi.org/10.1038/ngeo2695>

- 1188 Siegel, H., Gerth, M., Stottmeister, I., Baum, A., & Samiaji, J. (2019). Remote sensing of coastal discharge of SE
1189 Sumatra (Indonesia). In V. Barale & M. Gade (Eds.), *Remote Sensing of the Asian Seas* (pp. 359-376).
1190 Springer International Publishing. https://doi.org/10.1007/978-3-319-94067-0_20
- 1191 Siegel, H., Stottmeister, I., Reißmann, J., Gerth, M., Jose, C., & Samiaji, J. (2009). Siak River System — East-
1192 Sumatra: Characterisation of sources, estuarine processes, and discharge into the Malacca Strait. *Journal of*
1193 *Marine Systems*, 77(1), 148-159. <https://doi.org/https://doi.org/10.1016/j.jmarsys.2008.12.003>
- 1194 Spencer, R. G. M., Aiken, G. R., Butler, K. D., Dornblaser, M. M., Striegl, R. G., & Hernes, P. J. (2009). Utilizing
1195 chromophoric dissolved organic matter measurements to derive export and reactivity of dissolved organic
1196 carbon exported to the Arctic Ocean: A case study of the Yukon River, Alaska. *Geophysical Research Letters*,
1197 36(6). <https://doi.org/https://doi.org/10.1029/2008GL036831>
- 1198 Spencer, R. G. M., Butler, K. D., & Aiken, G. R. (2012). Dissolved organic carbon and chromophoric dissolved
1199 organic matter properties of rivers in the USA. *Journal of Geophysical Research: Biogeosciences*, 117(G3),
1200 n/a-n/a. <https://doi.org/10.1029/2011jg001928>
- 1201 Spencer, R. G. M., Hernes, P. J., Ruf, R., Baker, A., Dyda, R. Y., Stubbins, A., & Six, J. (2010). Temporal controls
1202 on dissolved organic matter and lignin biogeochemistry in a pristine tropical river, Democratic Republic of
1203 Congo. *Journal of Geophysical Research: Biogeosciences*, 115(G3).
1204 <https://doi.org/https://doi.org/10.1029/2009JG001180>
- 1205 Spencer, R. G. M., Stubbins, A., Hernes, P. J., Baker, A., Mopper, K., Aufdenkampe, A. K., et al. (2009).
1206 Photochemical degradation of dissolved organic matter and dissolved lignin phenols from the Congo River.
1207 *Journal of Geophysical Research: Biogeosciences*, 114(G3).
1208 <https://doi.org/https://doi.org/10.1029/2009JG000968>
- 1209 Stedmon, C. A., Amon, R. M. W., Rinehart, A. J., & Walker, S. A. (2011). The supply and characteristics of colored
1210 dissolved organic matter (CDOM) in the Arctic Ocean: Pan Arctic trends and differences. *Marine Chemistry*,
1211 124(1), 108-118. <https://doi.org/https://doi.org/10.1016/j.marchem.2010.12.007>
- 1212 Stedmon, C. A., & Bro, R. (2008). Characterizing dissolved organic matter fluorescence with parallel factor analysis:
1213 a tutorial. *Limnology and Oceanography: Methods*, 6(11), 572-579. <https://doi.org/10.4319/lom.2008.6.572>
- 1214 Stedmon, C. A., & Markager, S. (2005a). Resolving the variability in dissolved organic matter fluorescence in a
1215 temperate estuary and its catchment using PARAFAC analysis. *Limnology and Oceanography*, 50(2), 686-
1216 697. <https://doi.org/10.4319/lo.2005.50.2.0686>
- 1217 Stedmon, C. A., & Markager, S. (2005b). Tracing the production and degradation of autochthonous fractions of
1218 dissolved organic matter by fluorescence analysis. *Limnology and Oceanography*, 50(5), 1415-1426.
1219 <http://www.jstor.org/stable/3597686>
- 1220 Stedmon, C. A., Markager, S., & Bro, R. (2003). Tracing dissolved organic matter in aquatic environments using a
1221 new approach to fluorescence spectroscopy. *Marine Chemistry*, 82(3), 239-254.
1222 [https://doi.org/https://doi.org/10.1016/S0304-4203\(03\)00072-0](https://doi.org/https://doi.org/10.1016/S0304-4203(03)00072-0)
- 1223 Stedmon, C. A., & Nelson, N. B. (2015). Chapter 10 - The Optical Properties of DOM in the Ocean. In D. A. Hansell
1224 & C. A. Carlson (Eds.), *Biogeochemistry of Marine Dissolved Organic Matter (Second Edition)* (pp. 481-
1225 508). Academic Press. <https://doi.org/https://doi.org/10.1016/B978-0-12-405940-5.00010-8>
- 1226 Su, J., Cai, W.-J., Brodeur, J., Hussain, N., Chen, B., Testa, J. M., et al. (2020). Source partitioning of oxygen-
1227 consuming organic matter in the hypoxic zone of the Chesapeake Bay. *Limnology and Oceanography*, 65(8),
1228 1801-1817. <https://doi.org/https://doi.org/10.1002/lno.11419>
- 1229 Su, J., Dai, M., He, B., Wang, L., Gan, J., Guo, X., et al. (2017). Tracing the origin of the oxygen-consuming organic
1230 matter in the hypoxic zone in a large eutrophic estuary: the lower reach of the Pearl River Estuary, China.
1231 *Biogeosciences*, 14(18), 4085-4099. <https://doi.org/10.5194/bg-14-4085-2017>
- 1232 Susanto, R. D., Wei, Z., Adi, T. R., Zheng, Q., Fang, G., Fan, B., et al. (2016). Oceanography Surrounding Krakatau
1233 Volcano in the Sunda Strait, Indonesia. *Oceanography*, 29(2), 264-272.
1234 <http://www.jstor.org/stable/24862689>
- 1235 Urtizberea, A., Dupont, N., Rosland, R., & Aksnes, D. L. (2013). Sensitivity of euphotic zone properties to CDOM
1236 variations in marine ecosystem models. *Ecological Modelling*, 256, 16-22.
1237 <https://doi.org/https://doi.org/10.1016/j.ecolmodel.2013.02.010>
- 1238 Vähätalo, A. V., & Zepp, R. G. (2005). Photochemical Mineralization of Dissolved Organic Nitrogen to Ammonium
1239 in the Baltic Sea. *Environmental Science & Technology*, 39(18), 6985-6992.
1240 <https://doi.org/10.1021/es050142z>
- 1241 van Maren, D. S., & Gerritsen, H. (2012). Residual flow and tidal asymmetry in the Singapore Strait, with implications
1242 for resuspension and residual transport of sediment. *Journal of Geophysical Research: Oceans*, 117(C4).
1243 <https://doi.org/https://doi.org/10.1029/2011JC007615>

- 1244 Vantrepotte, V., Danhiez, F.-P., Loisel, H., Ouillon, S., Mériaux, X., Cauvin, A., & Dessailly, D. (2015). CDOM-
 1245 DOC relationship in contrasted coastal waters: implication for DOC retrieval from ocean color remote
 1246 sensing observation. *Optics Express*, 23(1), 33-54. <https://doi.org/10.1364/OE.23.000033>
- 1247 Vione, D., Lauri, V., Minero, C., Maurino, V., Malandrino, M., Carlotti, M. E., et al. (2009). Photostability and
 1248 photolability of dissolved organic matter upon irradiation of natural water samples under simulated sunlight.
 1249 *Aquatic Sciences*, 71(1), 34-45. <https://doi.org/10.1007/s00027-008-8084-3>
- 1250 Walker, S. A., Amon, R. M. W., & Stedmon, C. A. (2013). Variations in high-latitude riverine fluorescent dissolved
 1251 organic matter: A comparison of large Arctic rivers. *Journal of Geophysical Research: Biogeosciences*,
 1252 118(4), 1689-1702. <https://doi.org/https://doi.org/10.1002/2013JG002320>
- 1253 Ward, C. P., Nalven, S. G., Crump, B. C., Kling, G. W., & Cory, R. M. (2017). Photochemical alteration of organic
 1254 carbon draining permafrost soils shifts microbial metabolic pathways and stimulates respiration. *Nature*
 1255 *Communications*, 8(1), 772. <https://doi.org/10.1038/s41467-017-00759-2>
- 1256 Weishaar, J. L., Aiken, G. R., Bergamaschi, B. A., Fram, M. S., Fujii, R., & Mopper, K. (2003). Evaluation of specific
 1257 ultraviolet absorbance as an indicator of the chemical composition and reactivity of dissolved organic carbon.
 1258 *Environ Sci Technol*, 37(20), 4702-4708. <https://doi.org/10.1021/es030360x>
- 1259 Wilske, C., Herzsprung, P., Lechtenfeld, O. J., Kamjunke, N., & von Tümpling, W. (2020). Photochemically Induced
 1260 Changes of Dissolved Organic Matter in a Humic-Rich and Forested Stream. *Water*, 12(2), 331.
 1261 <https://www.mdpi.com/2073-4441/12/2/331>
- 1262 Wit, F., Rixen, T., Baum, A., Pranowo, W. S., & Hutahaean, A. A. (2018). The Invisible Carbon Footprint as a hidden
 1263 impact of peatland degradation inducing marine carbonate dissolution in Sumatra, Indonesia. *Scientific*
 1264 *Reports*, 8(1), 17403. <https://doi.org/10.1038/s41598-018-35769-7>
- 1265 Yamashita, Y., Fichot, C. G., Shen, Y., Jaffé, R., & Benner, R. (2015). Linkages among fluorescent dissolved organic
 1266 matter, dissolved amino acids and lignin-derived phenols in a river-influenced ocean margin [Original
 1267 Research]. *Frontiers in Marine Science*, 2(92). <https://doi.org/10.3389/fmars.2015.00092>
- 1268 Yamashita, Y., Jaffé, R., Maie, N., & Tanoue, E. (2008). Assessing the dynamics of dissolved organic matter (DOM)
 1269 in coastal environments by excitation emission matrix fluorescence and parallel factor analysis (EEM-
 1270 PARAFAC). *Limnology and Oceanography*, 53(5), 1900-1908. <https://doi.org/10.4319/lo.2008.53.5.1900>
- 1271 Yamashita, Y., & Tanoue, E. (2003). Chemical characterization of protein-like fluorophores in DOM in relation to
 1272 aromatic amino acids. *Marine Chemistry*, 82(3), 255-271. [https://doi.org/https://doi.org/10.1016/S0304-4203\(03\)00073-2](https://doi.org/https://doi.org/10.1016/S0304-4203(03)00073-2)
- 1273
- 1274 Yang, L., & Hur, J. (2014). Critical evaluation of spectroscopic indices for organic matter source tracing via end
 1275 member mixing analysis based on two contrasting sources. *Water Research*, 59, 80-89.
 1276 <https://doi.org/https://doi.org/10.1016/j.watres.2014.04.018>
- 1277 Ye, F., Guo, W., Wei, G., & Jia, G. (2018). The Sources and Transformations of Dissolved Organic Matter in the
 1278 Pearl River Estuary, China, as Revealed by Stable Isotopes. *Journal of Geophysical Research: Oceans*,
 1279 123(9), 6893-6908. <https://doi.org/https://doi.org/10.1029/2018JC014004>
- 1280 Zeebe, R. E., & Wolf-Gladrow, D. (2001). *CO2 in seawater: equilibrium, kinetics, isotopes*. Gulf Professional
 1281 Publishing.
- 1282 Zhou, Y., Evans, C. D., Chen, Y., Chang, K. Y. W., & Martin, P. (2021). Extensive Remineralization of Peatland-
 1283 Derived Dissolved Organic Carbon and Ocean Acidification in the Sunda Shelf Sea, Southeast Asia. *Journal*
 1284 *of Geophysical Research: Oceans*, 126(6), e2021JC017292.
 1285 <https://doi.org/https://doi.org/10.1029/2021JC017292>
- 1286 Zhou, Y., Martin, P., & Müller, M. (2019). Composition and cycling of dissolved organic matter from tropical
 1287 peatlands of coastal Sarawak, Borneo, revealed by fluorescence spectroscopy and parallel factor analysis.
 1288 *Biogeosciences*, 16(13), 2733-2749. <https://doi.org/10.5194/bg-16-2733-2019>
- 1289 Zhu, Z. Y., Oakes, J., Eyre, B., Hao, Y., Sia, E. S. A., Jiang, S., et al. (2020). The nonconservative distribution pattern
 1290 of organic matter in the Rajang, a tropical river with peatland in its estuary. *Biogeosciences*, 17(9), 2473-
 1291 2485. <https://doi.org/10.5194/bg-17-2473-2020>
- 1292 Zigah, P. K., McNichol, A. P., Xu, L., Johnson, C., Santinelli, C., Karl, D. M., & Repeta, D. J. (2017). Allochthonous
 1293 sources and dynamic cycling of ocean dissolved organic carbon revealed by carbon isotopes. *Geophysical*
 1294 *Research Letters*, 44(5), 2407-2415. <https://doi.org/https://doi.org/10.1002/2016GL071348>
- 1295 Zsolnay, A., Baigar, E., Jimenez, M., Steinweg, B., & Saccomandi, F. (1999). Differentiating with fluorescence
 1296 spectroscopy the sources of dissolved organic matter in soils subjected to drying. *Chemosphere*, 38(1), 45-
 1297 50. [https://doi.org/https://doi.org/10.1016/S0045-6535\(98\)00166-0](https://doi.org/https://doi.org/10.1016/S0045-6535(98)00166-0)
- 1298

JGR Biogeosciences

Supporting Information for

The validity of optical properties as tracers of terrigenous dissolved organic carbon during extensive remineralization in coastal waters

Yuan Chen¹, Patrick Martin¹, Yongli Zhou^{1, †}

¹ Asian School of the Environment, Nanyang Technological University, 639798, Singapore

[†] Present address: Marine Biological Laboratory, Woods Hole, MA 02543, USA

Contents of this file

Text S1

Figures S1 to S4

Tables S1 to S3

Introduction

The dataset contains previous data collected from Sarawak in north-western Borneo (Martin et al., 2018; Zhou et al., 2019), monthly data collected in the Singapore Strait, and experimental data for Singapore coastal water and a peatland-draining river water in Sarawak (partly published in Zhou et al. (2021)). Text S1 explains the calculation of the tDOC concentration and remineralized tDOC based on a two-endmember mixing model and a carbon isotope mass balance. Figure S1 shows a map of our study area. Figure S2 shows the derivation and validation of the riverine endmember value of a_{440} obtained from discharge-weighted average of four main rivers located on Sumatra (Siegel et al., 2019; Wit et al., 2018). Figure S3 presents fingerprints of five fluorescent components identified by parallel factor analysis (PARAFAC). Figure S4 shows that there is no relationship between dissolved organic matter optical properties and the extent of tDOC remineralization. Table S1 shows the parameter values used for the isotope mass balance calculation and the corresponding uncertainty calculation. Table S2 presents apparent and actual riverine endmember values from conservative mixing of remaining tDOC, total initial tDOC and timeseries a_{440} in the Singapore Strait, and discharge-weighted average a_{440} from data of four main rivers on Sumatra. Table S3 describes spectral characteristics and possible sources of the five PARAFAC components.

Text S1: Calculations of the remaining tDOC concentration and the amount of remineralized tDOC

S1.1 Remaining tDOC

We used a two-endmember isotope mixing model to calculate the concentration of tDOC in each sample, i.e., remaining tDOC concentration, from measured $\delta^{13}\text{C}_{\text{DOC}}$ and total DOC concentration. As our samples are the mixture of tDOC and marine DOC (mDOC), the measured DOC concentration and ^{13}C concentration are expressed as equations (Eqs.) S1–3:

$$[\text{DOC}]_{\text{meas}} = [\text{tDOC}] + [\text{mDOC}] \quad (\text{S1})$$

$$[\text{DO}^{13}\text{C}]_{\text{meas}} = [\text{DO}^{13}\text{C}]_{\text{tDOC}} + [\text{DO}^{13}\text{C}]_{\text{mDOC}} \quad (\text{S2})$$

$$[\text{DO}^{13}\text{C}]_{\text{meas}} = [\text{DOC}]_{\text{meas}} \times \frac{^{13}\text{C}}{^{12}\text{C} + ^{13}\text{C} + ^{14}\text{C}} \quad (\text{S3})$$

As ^{12}C accounts for >98.9% of total carbon in the natural environment, we can approximate:

$$\frac{^{13}\text{C}}{^{12}\text{C} + ^{13}\text{C} + ^{14}\text{C}} \approx \frac{^{13}\text{C}}{^{12}\text{C}} \quad (\text{S4})$$

$$\frac{^{12}\text{C}}{^{12}\text{C} + ^{13}\text{C} + ^{14}\text{C}} \approx 1 \quad (\text{S5})$$

Therefore, Eq. S3 is approximated as Eq. S6, in which the $^{13}\text{C}/^{12}\text{C}$ ratio (denoted as R) in the measured sample are calculated from measured $\delta^{13}\text{C}_{\text{DOC}}$ (Eq. S7):

$$[\text{DO}^{13}\text{C}]_{\text{meas}} \approx [\text{DOC}]_{\text{meas}} \times \mathbf{R}_{\text{meas}} \quad (\text{S6})$$

$$\mathbf{R}_{\text{meas}} = (\delta^{13}\text{C}_{\text{DOC-meas}}(\text{‰}) \div 1000 + 1) \times \mathbf{R}_{\text{VPDB}} \quad (\text{S7})$$

where the subscript “VPDB” denotes the international standard Vienna Pee Dee Belemnite ($\mathbf{R}_{\text{VPDB}} = 0.01123720$, IAEA (1993)).

Likewise, the concentrations of ^{13}C respectively contributed by tDOC and mDOC are approximated as Eqs. S8–9; R_{tDOC} and R_{mDOC} are calculated from $\delta^{13}\text{C}_{\text{DOC}}$ values of the riverine and marine endmember, respectively (Eqs. S10–11):

$$[\text{DO}^{13}\text{C}_{\text{tDOC}}] \approx [\text{tDOC}] \times R_{\text{tDOC}} \quad (\text{S8})$$

$$[\text{DO}^{13}\text{C}_{\text{mDOC}}] \approx [\text{mDOC}] \times R_{\text{mDOC}} \quad (\text{S9})$$

$$R_{\text{tDOC}} = (\delta^{13}\text{C}_{\text{DOC-riv}}(\text{‰}) \div 1000 + 1) \times R_{\text{VPDB}} \quad (\text{S10})$$

$$R_{\text{mDOC}} = (\delta^{13}\text{C}_{\text{DOC-mar}}(\text{‰}) \div 1000 + 1) \times R_{\text{VPDB}} \quad (\text{S11})$$

By applying Eq. S6 and S8–9 to Eq. S2, we have:

$$[\text{DOC}]_{\text{meas}} \times R_{\text{meas}} = [\text{tDOC}] \times R_{\text{tDOC}} + [\text{mDOC}] \times R_{\text{mDOC}} \quad (\text{S12})$$

Therefore, we calculated tDOC and mDOC concentrations in each sample by solving Eqs. S1, S7 and S10–12.

S1.2 Remineralized tDOC

For DIC, TA and $\delta^{13}\text{C}_{\text{DIC}}$, deviations between measured values and values predicted for conservative mixing are caused by photosynthesis/remineralization, CaCO_3 dissolution/calcification and CO_2 outgassing/uptake, in known stoichiometric proportions (Samanta et al., 2015; Zeebe & Wolf-Gladrow, 2001). Therefore, we firstly calculated the expected values for DIC, TA and $\delta^{13}\text{C}_{\text{DIC}}$ from conservative mixing and then estimated the amount of carbon that had undergone each biogeochemical processes from the difference between predicted and measured values and the stoichiometry of each process.

The fraction of river water (f_{riv}) and marine water (f_{mar}) was determined from salinity (Eqs. S1–3):

$$f_{\text{mar}} = \text{salinity}_{\text{meas}} \div \text{salinity}_{\text{mar}} \quad (\text{S13})$$

$$f_{\text{riv}} = 1 - f_{\text{mar}} \quad (\text{S14})$$

where the subscripts “mar”, “riv” and “meas” denote the marine and riverine endmembers, and measured data, respectively.

Expected values for DIC, TA, DI¹²C and DI¹³C from conservative mixing were calculated as:

$$\mathbf{Var}_{\text{mix}} = \mathbf{Var}_{\text{riv}} \times \mathbf{f}_{\text{riv}} + \mathbf{Var}_{\text{mar}} \times \mathbf{f}_{\text{mar}} \quad (\text{S15})$$

where “Var” stands for the variables DIC, TA, DI¹²C and DI¹³C, and the subscript “mix” denotes values expected from conservative mixing.

To calculate conservative mixing $\delta^{13}\text{C}_{\text{DIC}}$ values, we followed the approximation in Eqs. S4–5 and S8–11, and riverine and marine endmember values for DI¹²C and DI¹³C were calculated from Eqs. S16–17:

$$[\text{DI}^{13}\text{C}]_{\text{end}} \approx [\text{DIC}]_{\text{end}} \times \mathbf{R}_{\text{end}} \quad (\text{S16})$$

$$[\text{DI}^{12}\text{C}]_{\text{end}} \approx [\text{DIC}]_{\text{end}} \times \mathbf{1} \quad (\text{S17})$$

where the subscript “end” denotes riverine/marine endmembers.

Combined with $[\text{DI}^{12}\text{C}]_{\text{mix}}$ and $[\text{DI}^{13}\text{C}]_{\text{mix}}$ from Eq. S15, $\delta^{13}\text{C}_{\text{DIC-mix}}$ was calculated following Eqs. S18–19:

$$\mathbf{R}_{\text{mix}} = \frac{[\text{DI}^{13}\text{C}]_{\text{mix}}}{[\text{DI}^{12}\text{C}]_{\text{mix}}} \quad (\text{S18})$$

$$\delta^{13}\text{C}_{\text{DIC-mix}}(\text{‰}) = \frac{\mathbf{R}_{\text{mix}} - \mathbf{R}_{\text{VPDB}}}{\mathbf{R}_{\text{VPDB}}} \times \mathbf{1000} \quad (\text{S19})$$

Taking all the physical and biogeochemical processes and their stoichiometric effect into account, which can be derived from the slopes in a TA against DIC plot (Zeebe & Wolf-Gladrow, 2001; Zhou et al., 2021), the measured DIC and TA are expressed as:

$$\text{DIC}_{\text{meas}} = \text{DIC}_{\text{mix}} + (+1) \times \mathbf{M}_{\text{rem}} + (+1) \times \mathbf{M}_{\text{diss}} + (-1) \times \mathbf{M}_{\text{outg}} \quad (\text{S20})$$

$$\text{TA}_{\text{meas}} = \text{TA}_{\text{mix}} + (-0.025) \times \mathbf{M}_{\text{rem}} + (+2) \times \mathbf{M}_{\text{diss}} + 0 \times \mathbf{M}_{\text{outg}} \quad (\text{S21})$$

where M represents the molar contribution of different processes, and the subscripts “rem”, “diss” and “outg” denote tDOC remineralization/primary production, CaCO₃ dissolution/production and CO₂ outgassing/uptake, respectively.

The impacts of tDOC remineralization, calcium carbonate dissolution and CO₂ outgassing on $\delta^{13}\text{C}_{\text{DIC}}$ were estimated according to Samanta et al. (2015):

$$\Delta\delta^{13}\text{C}_{\text{DIC-rem}} \approx \frac{M_{\text{rem}}}{\text{DIC}_{\text{mix}}} \times (\delta^{13}\text{C}_{\text{tDIC}} - \delta^{13}\text{C}_{\text{DIC-mix}}) \quad (\text{S22})$$

$$\Delta\delta^{13}\text{C}_{\text{DIC-diss}} \approx \frac{M_{\text{diss}}}{\text{DIC}_{\text{mix}}} \times (\delta^{13}\text{C}_{\text{DIC-diss}} - \delta^{13}\text{C}_{\text{DIC-mix}}) \quad (\text{S23})$$

$$\Delta\delta^{13}\text{C}_{\text{DIC-outg}} \approx \frac{-M_{\text{outg}}}{\text{DIC}_{\text{mix}}} \times 10^3 \times (\alpha_{\text{CO}_2} - 1) \quad (\text{S24})$$

where the symbol “ Δ ” represents the deviation between measured data and values expected from conservative mixing caused by each process; $\delta^{13}\text{C}_{\text{tDIC}}$ is the $\delta^{13}\text{C}$ of DIC produced by tDOC remineralization, which we take as -32‰ (see Section 2.5.2) $\delta^{13}\text{C}_{\text{DIC-diss}}$ is the $\delta^{13}\text{C}$ of DIC produced by carbonate dissolution, reported as 0‰ (Samanta et al., 2015; Su et al., 2019); α_{CO_2} is the fractionation factor between air and sea surface, and is calculated from the in-situ temperature and the approximation (Rau et al., 1996; Zeebe & Wolf-Gladrow, 2001; Zhou et al., 2021):

$$\epsilon_{\text{CO}_2} = 23.644 - 9701.5 \div T(\text{K}) \quad (\text{S25})$$

$$\epsilon_{\text{CO}_2} \approx 10^3 \times \ln \alpha_{\text{CO}_2} \approx 10^3 \times (\alpha_{\text{CO}_2} - 1) \quad (\text{S26})$$

Then, the measured $\delta^{13}\text{C}_{\text{DIC}}$ is expressed as the combination of physical mixing and these biogeochemical processes:

$$\begin{aligned} \delta^{13}\text{C}_{\text{DIC-meas}}(\text{‰}) &= \delta^{13}\text{C}_{\text{DIC-mix}}(\text{‰}) + \frac{M_{\text{rem}}}{\text{DIC}_{\text{mix}}} \times (\delta^{13}\text{C}_{\text{tDIC}} - \delta^{13}\text{C}_{\text{DIC-mix}}) + \frac{M_{\text{diss}}}{\text{DIC}_{\text{mix}}} \times \\ &(\delta^{13}\text{C}_{\text{DIC-diss}} - \delta^{13}\text{C}_{\text{DIC-mix}}) + \frac{-M_{\text{outg}}}{\text{DIC}_{\text{mix}}} \times 10^3 \times (\alpha_{\text{CO}_2} - 1) \end{aligned} \quad (\text{S27})$$

By solving Eqs. S20–21 and 27, M_{rem} , M_{diss} and M_{outg} were calculated. Further details of the derivation and approximation can be found in Zhou et al. (2021).

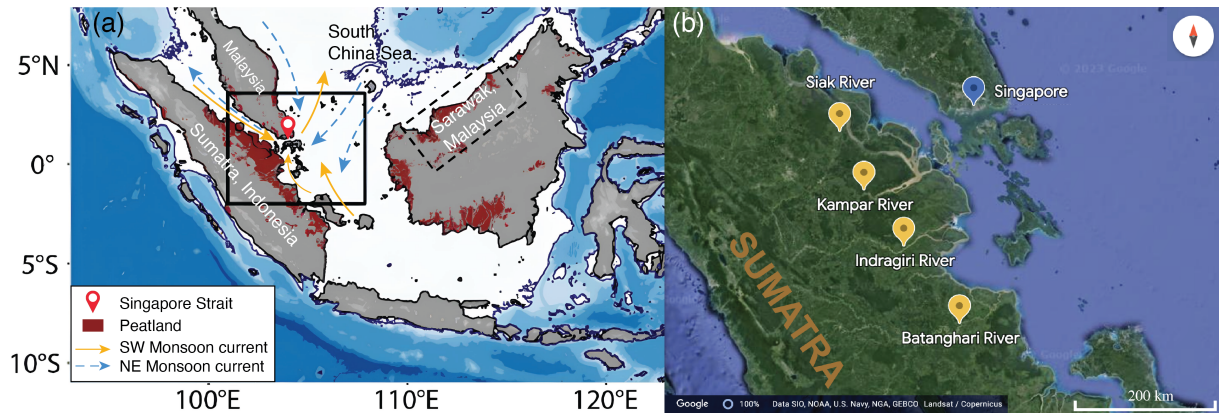


Figure S1. (a) Regional map showing our sampling sites (Singapore Strait and Sarawak) and the monsoon-driven reversal in ocean currents (arrows). (b) Locations of the four peatland-draining rivers (Siak, Kampar, Indragiri and Batanghari) that represent the most plausible main source of tDOC input to the Singapore Strait, and which we used to estimate riverine endmember values.

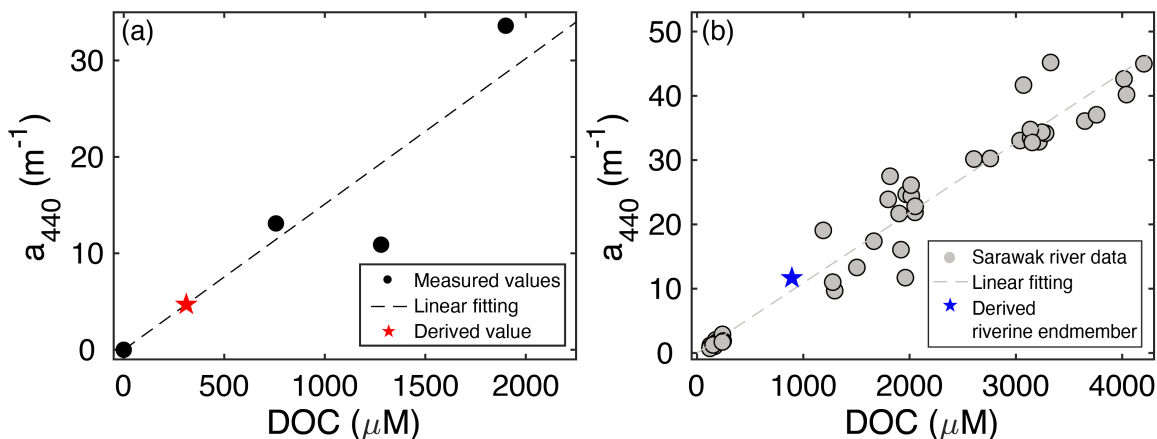


Figure S2. (a) Relationship between average a_{440} and DOC concentration for the four main peatland-draining rivers on Sumatra (Indragiri, Kampar, Siak and Batanghari; data from (Siegel et al., 2019; Wit et al., 2018)). Note that for the Batanghari river there is no published a_{440} , so the Batanghari a_{440} was estimated based on the a_{440} –DOC relationship of the other rivers (red star; relationship forced through the origin). (b) Based on the a_{440} and DOC concentrations in panel (a) and the river discharge data in Wit et al. (2018), we calculated a discharge-weighted average a_{440} and DOC concentration for the four Sumatran rivers as estimated mean riverine endmember values (blue star) for the peatland DOM input to the Singapore Strait. This estimated average riverine a_{440} and DOC for Sumatra falls very close to the relationship of a_{440} to DOC observed for river data measured in Sarawak (Martin et al., 2018).

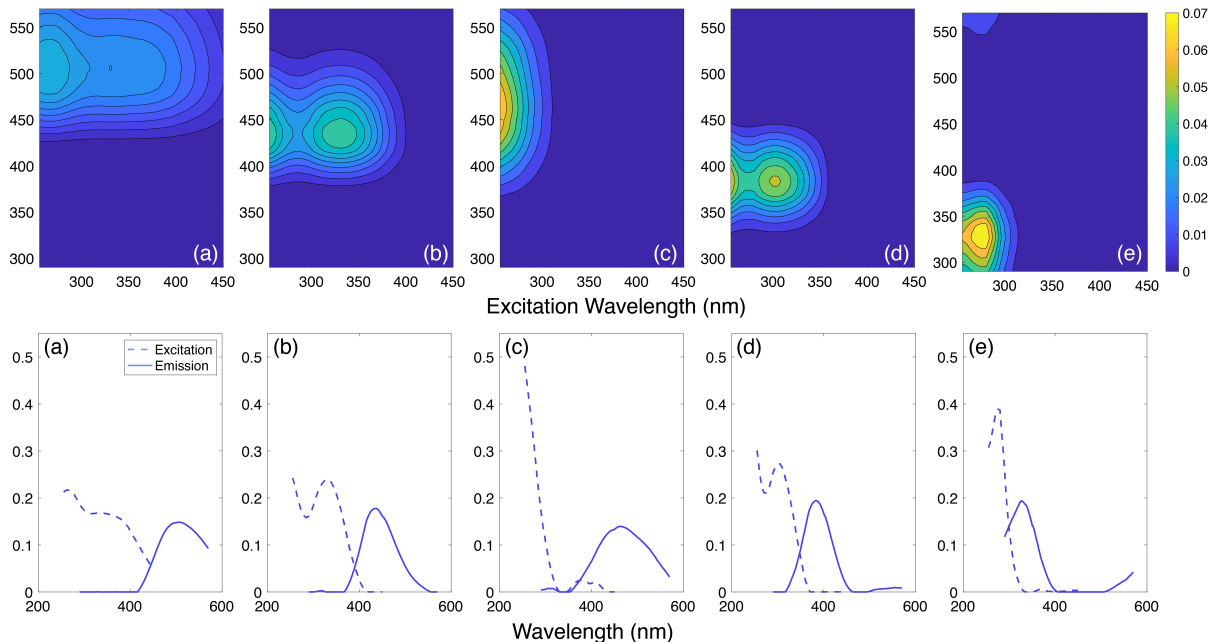


Figure S3. Components revealed by PARAFAC analysis of our combined FDOM dataset; top row shows excitation-emission plots and bottom row shows the corresponding excitation and emission spectra (components 1–5 are ordered left-to-right).

Table S1. Spectral characteristics of the five components identified by PARAFAC analysis for our combined FDOM dataset, and interpretation of possible sources of each compound based on previous literature.

Component	Ex_{max} (nm)	Em_{max} (nm)	Description and probable source	References
C1	265 (330)	506	Soil fulvic acid, common to a wide range of freshwater	(Osburn et al., 2016; Stedmon & Markager, 2005a; Stedmon et al., 2003)
C2	<255 (330)	436	Humic fluorophore group, highest concentration in forest stream and wetlands	(Stedmon & Markager, 2005a; Stedmon et al., 2003)
C3	<255	462	Terrestrial humic substances	(Coble, 1996; Osburn et al., 2016; Stedmon et al., 2003)
C4	<255 (300)	384	Protein-like materials; terrestrial humic materials; possible microbial processed	(Cory & McKnight, 2005; Stedmon & Markager, 2005b; Stedmon et al., 2003; Zhou et al., 2019)
C5	275	326	Non-humic-like materials, autochthonous DOM, tryptophan-like components	(Du et al., 2016; Murphy et al., 2008; Osburn et al., 2016)

Table S2. Endmember values and their uncertainties for all parameters used to calculate the remaining tDOC and total initial tDOC concentrations. Uncertainties for each parameter for the riverine and marine endmembers represent 1 standard deviation and were used to estimate the overall uncertainty for remaining and total initial tDOC using a Monte Carlo Simulation. Analytical uncertainties for each parameter are also given (1 standard deviation).

Parameter	Riverine endmember ^a	Marine endmember	Uncertainty of measurements
Salinity	0	32.56 ± 0.37	± 0.01
DIC (μmol kg ⁻¹)	453 ± 34	1901 ± 14	± 0.15%
TA (μmol kg ⁻¹)	310 ± 34	2159 ± 17	± 0.13%
δ ¹³ C _{DIC} (‰)	-15.32 ± 1	-0.23 ± 0.10	± 0.2
δ ¹³ C _{DOC} (‰)	-29 ± 1	-21.39 ± 1.71	± 0.2
δ ¹³ C _{tDIC} (‰)	-32 ± 1	-	-

^a Discharge-weighted average of published data (Siegel et al., 2019; Wit et al., 2018)

Table S3. Apparent and actual riverine endmember values for remaining and total initial tDOC and for remaining CDOM a_{440} were estimated by extrapolating linear regressions for each parameter versus salinity back to salinity 0, using the Singapore Strait time series data. The total initial a_{440} was estimated as the discharge-weighted average a_{440} from the published river data from Sumatra (see Figure S2).

Parameter used to calculate riverine endmember	Riverine endmember value	Uncertainty	Loss percent
Remaining tDOC (μmol L ⁻¹) ^a	389	± 97	-
Total initial tDOC (μmol L ⁻¹) ^a	814	± 133	55.5%
Remaining CDOM (a_{440} , m ⁻¹) ^a	2.72	± 0.18	-
Total initial CDOM (a_{440} , m ⁻¹) ^b	11.67	± 0.90	76.5%

^a Apparent conservative mixing of timeseries data in the Singapore Strait

^b Discharge-weighted average of four main rivers located on Sumatra (Siegel et al., 2019; Wit et al., 2018)

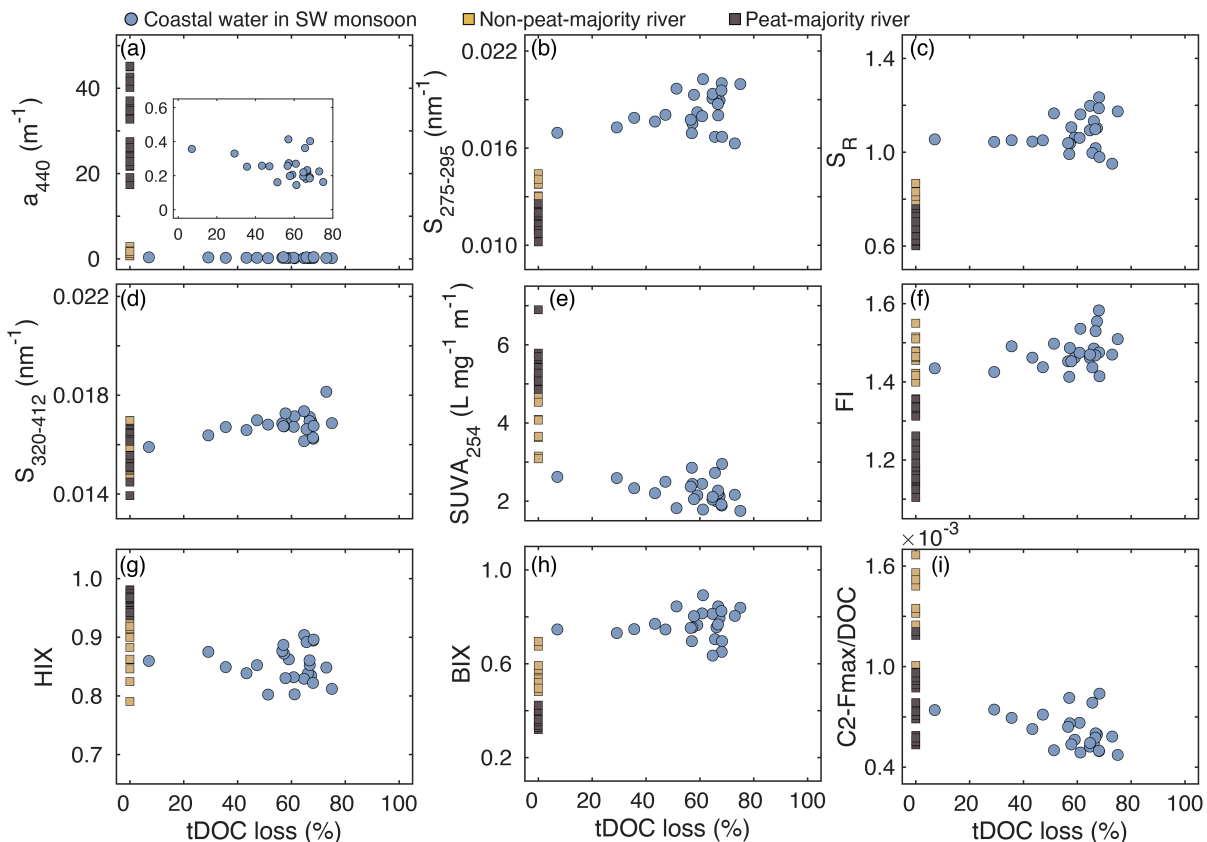


Figure S4. The relationship between optical properties and percentage tDOC remineralization (as calculated from the proportion of remineralized tDOC relative to total initial tDOC based on the carbon stable isotope mass balance). Coastal water data from the Singapore Strait are shown in blue circles (SW Monsoon season only) while Sarawak river data are showed in light and dark brown squares for rivers with, respectively, <50% and >50% peatland coverage in their catchments. We found no significant correlations for the Singapore data, indicating that these optical properties may not be able to quantify the extent of tDOC remineralization.

Data Set S1. Compiled dataset including multi-year time series (from Oct-2017 to Jul-2021) of DOC concentration, stable carbon isotope composition, and optical properties collected in the Singapore Strait, environmental data collected from three expeditions in Sarawak, Borneo and experimental data from photo- and biodegradation incubations for peatland-draining river water and coastal seawater.

References

- Coble, P. G. (1996). Characterization of marine and terrestrial DOM in seawater using excitation-emission matrix spectroscopy. *Marine Chemistry*, 51(4), 325-346. [https://doi.org/https://doi.org/10.1016/0304-4203\(95\)00062-3](https://doi.org/https://doi.org/10.1016/0304-4203(95)00062-3)
- Cory, R. M., & McKnight, D. M. (2005). Fluorescence spectroscopy reveals ubiquitous presence of oxidized and reduced quinones in dissolved organic matter. *Environmental Science & Technology*, 39(21), 8142-8149. <https://doi.org/10.1021/es0506962>
- Du, Y., Zhang, Y., Chen, F., Chang, Y., & Liu, Z. (2016). Photochemical reactivities of dissolved organic matter (DOM) in a sub-alpine lake revealed by EEM-PARAFAC: An insight into the fate of allochthonous DOM in alpine lakes affected by climate change. *Science of The Total Environment*, 568, 216-225. <https://doi.org/https://doi.org/10.1016/j.scitotenv.2016.06.036>
- Martin, P., Cherukuru, N., Tan, A. S. Y., Sanwlani, N., Mujahid, A., & Müller, M. (2018). Distribution and cycling of terrigenous dissolved organic carbon in peatland-draining rivers and coastal waters of Sarawak, Borneo. *Biogeosciences*, 15(22), 6847-6865. <https://doi.org/10.5194/bg-15-6847-2018>
- Murphy, K. R., Stedmon, C. A., Waite, T. D., & Ruiz, G. M. (2008). Distinguishing between terrestrial and autochthonous organic matter sources in marine environments using fluorescence spectroscopy. *Marine Chemistry*, 108(1), 40-58. <https://doi.org/https://doi.org/10.1016/j.marchem.2007.10.003>
- Osburn, C. L., Boyd, T. J., Montgomery, M. T., Bianchi, T. S., Coffin, R. B., & Paerl, H. W. (2016). Optical proxies for terrestrial dissolved organic matter in estuaries and coastal Waters [Original Research]. *Frontiers in Marine Science*, 2(127). <https://doi.org/10.3389/fmars.2015.00127>
- Rau, G. H., Riebesell, U., & Wolf-Gladrow, D. (1996). A model of photosynthetic ^{13}C fractionation by marine phytoplankton based on diffusive molecular CO_2 uptake. *Marine Ecology Progress Series*, 133, 275-285. <https://www.int-res.com/abstracts/meps/v133/p275-285/>
- Samanta, S., Dalai, T. K., Pattanaik, J. K., Rai, S. K., & Mazumdar, A. (2015). Dissolved inorganic carbon (DIC) and its $\delta^{13}\text{C}$ in the Ganga (Hooghly) River estuary, India: Evidence of DIC generation via organic carbon degradation and carbonate dissolution. *Geochimica et Cosmochimica Acta*, 165, 226-248. <https://doi.org/https://doi.org/10.1016/j.gca.2015.05.040>
- Siegel, H., Gerth, M., Stottmeister, I., Baum, A., & Samiaji, J. (2019). Remote sensing of coastal discharge of SE Sumatra (Indonesia). In V. Barale & M. Gade (Eds.), *Remote Sensing of the Asian Seas* (pp. 359-376). Springer International Publishing. https://doi.org/10.1007/978-3-319-94067-0_20
- Stedmon, C. A., & Markager, S. (2005a). Resolving the variability in dissolved organic matter fluorescence in a temperate estuary and its catchment using PARAFAC analysis. *Limnology and Oceanography*, 50(2), 686-697. <https://doi.org/10.4319/lo.2005.50.2.0686>
- Stedmon, C. A., & Markager, S. (2005b). Tracing the production and degradation of autochthonous fractions of dissolved organic matter by fluorescence analysis. *Limnology and Oceanography*, 50(5), 1415-1426. <http://www.jstor.org/stable/3597686>

- Stedmon, C. A., Markager, S., & Bro, R. (2003). Tracing dissolved organic matter in aquatic environments using a new approach to fluorescence spectroscopy. *Marine Chemistry*, 82(3), 239-254. [https://doi.org/https://doi.org/10.1016/S0304-4203\(03\)00072-0](https://doi.org/https://doi.org/10.1016/S0304-4203(03)00072-0)
- Su, J., Cai, W.-J., Hussain, N., Brodeur, J., Chen, B., & Huang, K. (2019). Simultaneous determination of dissolved inorganic carbon (DIC) concentration and stable isotope ($\delta^{13}\text{C}$ -DIC) by Cavity Ring-Down Spectroscopy: Application to study carbonate dynamics in the Chesapeake Bay. *Marine Chemistry*, 215, 103689. <https://doi.org/https://doi.org/10.1016/j.marchem.2019.103689>
- Wit, F., Rixen, T., Baum, A., Pranowo, W. S., & Hutahaean, A. A. (2018). The Invisible Carbon Footprint as a hidden impact of peatland degradation inducing marine carbonate dissolution in Sumatra, Indonesia. *Scientific Reports*, 8(1), 17403. <https://doi.org/10.1038/s41598-018-35769-7>
- Zeebe, R. E., & Wolf-Gladrow, D. (2001). *CO₂ in seawater: equilibrium, kinetics, isotopes*. Gulf Professional Publishing.
- Zhou, Y., Evans, C. D., Chen, Y., Chang, K. Y. W., & Martin, P. (2021). Extensive Remineralization of Peatland-Derived Dissolved Organic Carbon and Ocean Acidification in the Sunda Shelf Sea, Southeast Asia. *Journal of Geophysical Research: Oceans*, 126(6), e2021JC017292. <https://doi.org/https://doi.org/10.1029/2021JC017292>
- Zhou, Y., Martin, P., & Müller, M. (2019). Composition and cycling of dissolved organic matter from tropical peatlands of coastal Sarawak, Borneo, revealed by fluorescence spectroscopy and parallel factor analysis. *Biogeosciences*, 16(13), 2733-2749. <https://doi.org/10.5194/bg-16-2733-2019>